

Development and Validation of a TRNSYS Type to Simulate Heat Pipe Heat Exchangers in Transient Applications of Waste Heat Recovery

Daniel Brough^a, João Ramos^b, Bertrand Delpech^a, Hussam Jouhara^{a*}

a- Heat Pipe and Thermal Management Research Group, Brunel University London, Uxbridge, Middlesex, UB8 3PH, London, UK.

b- Faculty of Computing Engineering and Science, University of South Wales, Pontypridd, CF37 1DL, UK.

*- Corresponding Author. Email address: hussam.jouhara@brunel.ac.uk (H. Jouhara).

ABSTRACT

Heat pipe heat exchangers (HPHEs) are being more frequently used in energy intensive industries as a method of low-grade waste heat recovery. Prior to the installation of a HPHE, the effect of the heat exchanger within the system requires modelling to simulate the overall impact. From this, potential savings and emission reductions can be determined, and the utilisation of the waste heat can be optimised. One such simulation software is TRNSYS. Currently available heat exchanger simulation components in TRNSYS use averaged values such as a constant effectiveness, constant heat transfer coefficient or conductance for the inputs, which are fixed during the entire simulation. These predictions are useful in a steady-state controlled temperature environment such as a heat treatment facility, but not optimal for the majority of energy recovery applications which operate with fluctuating conditions. A transient TRNSYS HPHE component has been developed using the Effectiveness-Number of Transfer Units (ϵ -NTU) method and validated against experimental results. The model predicts outlet temperatures and energy recovery well within an accuracy of 15% and an average of 4.4% error when compared to existing experimental results, which is acceptable for engineering applications.

Keywords: Heat Pipe Heat Exchanger, Waste Heat Recovery; Transient Modelling; System Simulation; TRNSYS

Nomenclature

Acronyms

| Symbol | Description |
|-----------------|--|
| ϵ -NTU | Effectiveness - Number of Transfer Units |
| DLL | Dynamic Link Library |
| EU | European Union |
| Fortran | FORmula TRANslation |
| GDP | Gross Domestic Product |
| HPHE | Heat Pipe Heat Exchanger |
| LMTD | Log Mean Temperature Difference |
| TRNSYS | TRaNsient SYstems Simulation |
| WHR | Waste Heat Recovery |

Symbols and Units

| Symbol | Description | Unit |
|-----------|---|----------------------------------|
| A | Overall heat transfer area | m^2 |
| C | Heat capacity | J.K^{-1} |
| c_p | Specific heat capacity | $\text{J.kg}^{-1}.\text{K}^{-1}$ |
| D_o | Outer diameter (of tube) | m |
| e | Thickness | m |
| F_a | Correction factor associated with arrangement | Dimensionless |
| H | Width | m |
| h | Heat transfer coefficient | $\text{W.m}^{-2}.\text{K}^{-1}$ |
| h_{fg} | Latent heat | J.kg^{-1} |
| k | Thermal conductivity | $\text{W.m}^{-1}.\text{K}^{-1}$ |
| K | Constant | Dimensionless |
| L_{ch} | Characteristic length | m |
| \dot{m} | Mass flow rate | kg.s^{-1} |
| P | Pitch | m |
| Pr | Prandtl number | Dimensionless |
| Nu | Nusselt number | Dimensionless |
| N_r | Number of longitudinal rows of heat pipes | Dimensionless |

| | | |
|-----------|--|-------------------|
| N_t | Number of heat pipes in a transverse row | Dimensionless |
| R | Thermal resistance | $K.W^{-1}$ |
| Re | Reynolds number | Dimensionless |
| T | Temperature | $^{\circ}C$ |
| u | Flow velocity | $m.s^{-1}$ |
| V_{max} | Maximum velocity across tube bundle | $m.s^{-1}$ |
| U | Overall heat transfer coefficient | $W.m^{-2}.K^{-1}$ |
| v_f | Free stream velocity | $m.s^{-1}$ |
| A_{min} | Location of minimum free flow area | m^2 |
| S_L | Longitudinal row pitch | m |
| S'_L | Diagonal row pitch | m |
| S_T | Transverse row pitch | m |
| \dot{Q} | Heat transfer rate | kW |

Greek symbols

| Symbol | Description | Unit |
|---------------|--|---------------|
| α | Thermal diffusivity | $m^2.s^{-1}$ |
| Δ | Difference | Dimensionless |
| ε | Effectiveness | Dimensionless |
| η | Efficiency | Dimensionless |
| μ | Dynamic viscosity | $N.s.m^{-2}$ |
| ν | Kinematic viscosity (momentum diffusivity) | $m^2.s^{-1}$ |
| ρ | Density | $kg.m^{-3}$ |
| σ | Surface tension | $N.m^{-2}$ |
| Φ | Figure of merit | $W.m^{-2}$ |

Subscripts and superscripts

| Symbol | Description |
|--------|----------------------------------|
| act | Actual |
| b | Boiling |
| c | Condenser |
| cd | Condensation |
| D | Associated with diameter of pipe |

| | |
|------------|-------------------------------|
| <i>e</i> | Evaporator |
| <i>f</i> | Fin |
| <i>fc</i> | Forced convection |
| <i>h</i> | Convection |
| <i>hl</i> | Helical |
| <i>hp</i> | Heat pipe |
| <i>in</i> | Inlet |
| <i>k</i> | Conduction |
| <i>l</i> | Liquid |
| <i>LM</i> | Logarithmic mean |
| <i>max</i> | Maximum |
| <i>min</i> | Minimum |
| <i>n</i> | Associated with a row |
| <i>o</i> | Outer |
| <i>out</i> | Outlet |
| <i>s</i> | Associated with external wall |
| <i>t</i> | Thermosyphon |
| <i>tot</i> | Total |

1 Introduction

Energy is a central topic of conversation of many developed nations, particularly the overreliance on fossil fuels for energy production. Global energy consumption keeps increasing as the world population and the needs of its people increase, but its source may be shifting. So far, petroleum consumption around the world has been steadily increasing ever since its inception, and consequently, mounting greenhouse gas emissions [1]. Simultaneously, the current zeitgeist is that of a green, carbon-neutral planet which pushes for more sustainable sources of energy, either from harnessing renewable energies but additionally by improving the heat recovery of existing systems. At the 2019 United Nations Climate Change Summit, it was announced that countries around the world should reduce emissions by 45% by 2030 on the way to net zero carbon emissions by 2050 [2]. This is a follow up to the 2016 Paris Agreement [3], and has been reinforced by European Union (EU) 2030 energy targets [4], which aim to reduce greenhouse gas emissions to 80-95% below 1990 levels by 2050. Further information on European and UK regulatory frameworks and policies on energy efficiency, in industry, are provided within Ref. [5].

The industrial sector contributes 30.5 % of the total worldwide GDP [6] whilst also being accountable for 33% of the total greenhouse gas emissions [7]. One way to reduce this contribution is by upgrading or retrofitting inefficient plants with modern technology. One of the methods used is Waste Heat Recovery (WHR) by way of heat exchangers, as it has been reported that 70% of global energy demand in the industrial sector is for heat or thermal processes [8], 72% in the United Kingdom [7].

A heat exchanger is a device whose purpose is to transfer heat energy between two or more fluids. As previously mentioned, a growing area of interest for heat exchangers is the recovery of waste heat [9]. Waste heat is defined as any heat produced by a machine or as a by-product of an industrial process that is lost to atmosphere and has the potential to be captured or reused. A subset of heat exchangers used as WHR devices are heat exchangers equipped with heat pipes (a Heat Pipe Heat Exchanger or HPHE).

Wickless heat pipes, also known as thermosyphons or gravity-assisted heat pipes, are passive heat recovery devices [10]. They consist of hollow tubes partially filled with a working fluid in both liquid and vapour phase. As heat is applied to the pool of fluid at the bottom half of the pipe, termed evaporator, the fluid evaporates and, in gaseous form, travels to the top of the pipe. By having a colder stream make contact with the top section of the pipe, the cooler walls at the top of the heat pipe cause the fluid to condense and, due to the action of gravity, travel back to the bottom of the heat pipe in liquid form (Figure 1). This is a continuous process that takes place as long as there is a temperature difference between the evaporator and the condenser of the heat pipe. When working at full capacity, if there are no non-condensable gases present inside the heat pipe, it operates nearly isothermally, with little difference in temperature between the top and bottom of the heat pipe. This is also the reason the heat pipe is often referred to as a superconductor.

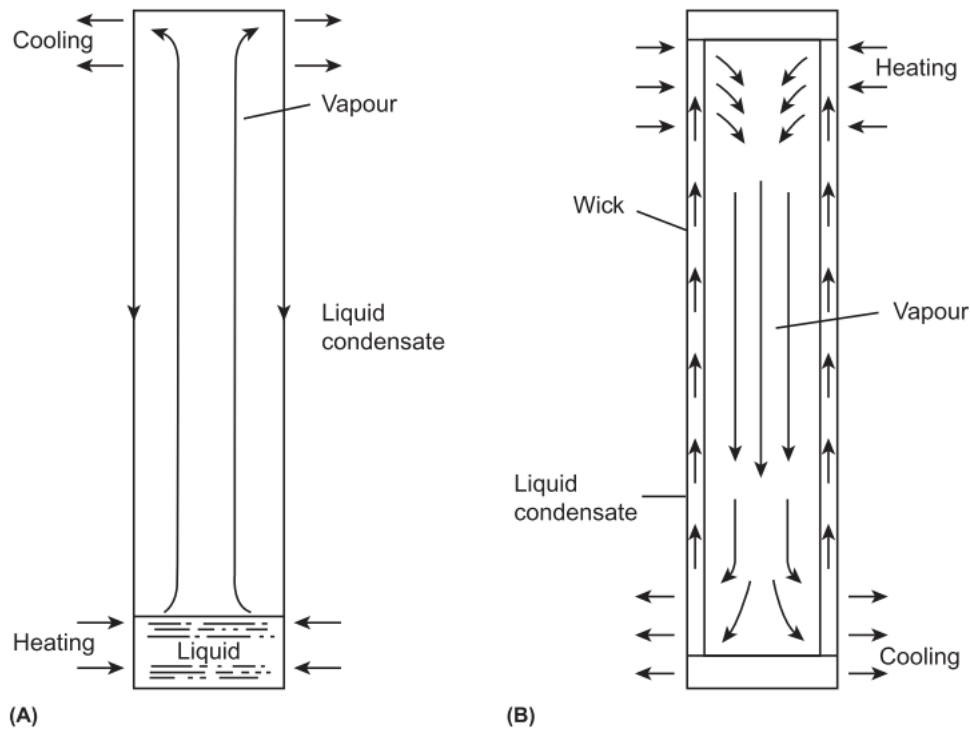


Figure 1: Thermosyphon (A) and Heat pipe (B) operating principle [10].

Some heat pipes are equipped with an inner wick structure which allows them to function against the force of gravity. Historically, this was when heat pipes first started gaining popularity as useful heat sinks for space applications or small electronic devices [11]. Throughout this paper, the heat pipes referred to are wickless heat pipes. A HPHE uses bundles of these heat pipes with the evaporator section in contact with a hot stream and the condenser section in contact with the cooler stream, isolated by a separation plate.

This paper provides a literature review, outlines previous simulations conducted, and shows how an improved simulation methodology has been developed using TRNSYS software to simulate a HPHE's performance transiently by creating a dedicated HPHE component, which provides accurate predictions on outlet temperatures and energy recovery. A full-scale working HPHE unit installed to recover waste heat from a continuous roller kiln that fires ceramic tiles has been used to empirically validate the model.

2 Literature Review

2.1 Industrial Applications

When looking at heat recovery applications, the main advantage of a HPHE over traditional heat exchangers is their superior flow separation and increased redundancy as each pipe functions as an individual heat exchanger. This means that if one pipe fails, it will not put the integrity or overall performance of the heat exchanger at risk and, importantly, prevents any cross-contamination between heat streams. This is crucial when contamination between streams is undesirable. Heat pipes also have a high effective thermal conductivity compared with traditional heat exchangers due to the two-phase boiling and condensation heat transfer, which allows its heat transfer coefficient to be directly correlated with the specific heat of the working fluid being used. Heat transfer coefficients in the magnitude of 10^3 - 10^5 $\text{W}\cdot\text{m}^{-2}\cdot\text{K}^{-1}$ have been reported [12].

In heat exchangers, counter-flow is usually preferable to parallel-flow. Heat transfer is a function of temperature difference, and counter-flow allows for a continuous difference in temperature between the two streams. The difference in temperature between the evaporator and the condenser is also an operating requirement in a heat pipe. Therefore, in a HPHE, the designer must ensure that each heat pipe is located between two flows at different temperatures, thus consistently having a difference in temperature (ΔT) between its ends. Furthermore, in counter-flow, the temperature of the hot outlet stream can be lower than the cold sink outlet stream. A counter-flow HPHE and a comparison between parallel and counter-flow is shown in Figure 2. The component created in this paper was to replicate a counter-flow HPHE.

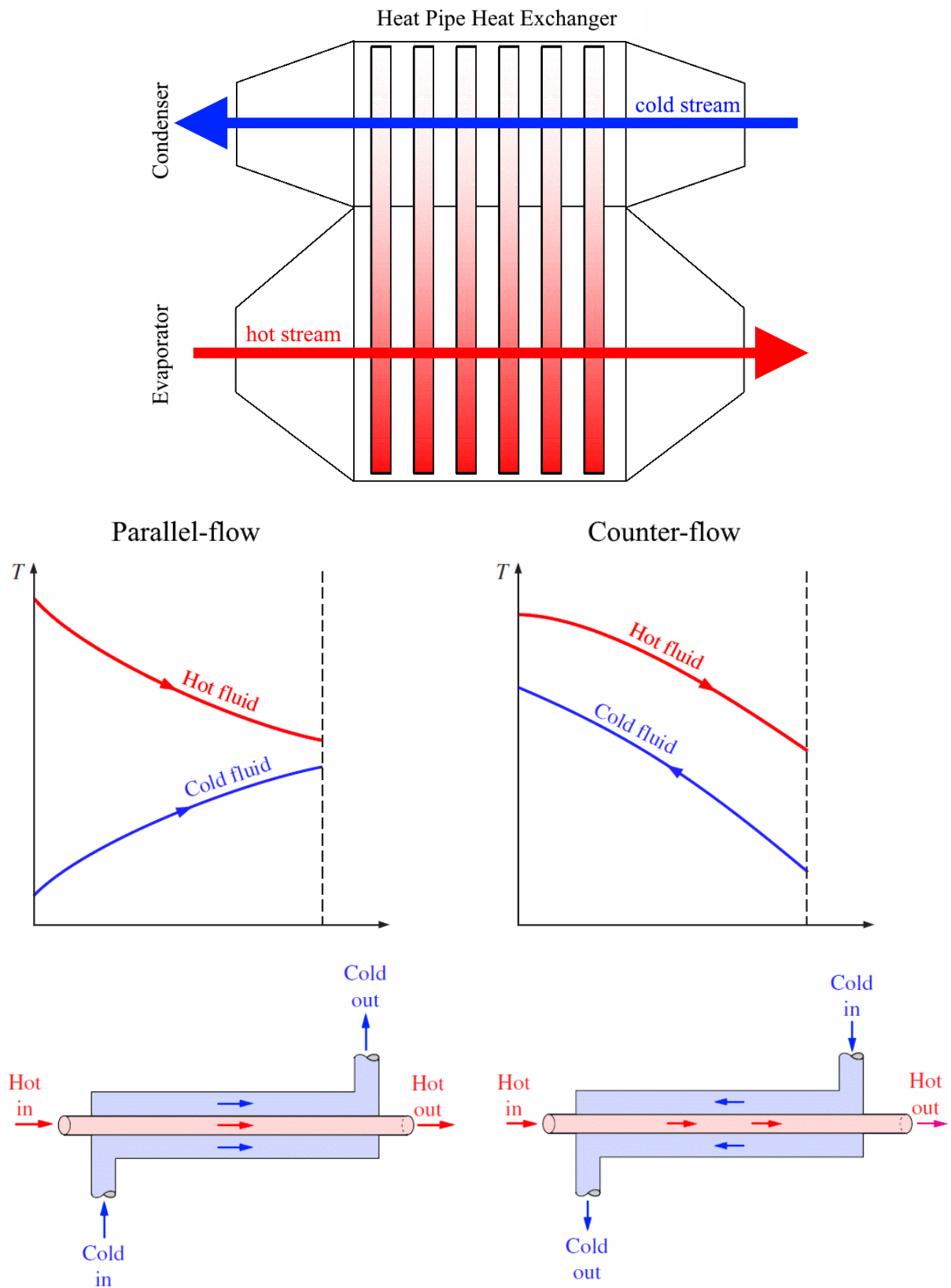


Figure 2: Counter-flow heat pipe heat exchanger with flow comparison. Adapted from [13].

In most applications, a HPHE is defined as a counter-flow heat exchanger as a whole, but in essence it is a combination of two crossflow heat exchangers if divided between evaporator and condenser: counter-flow due to the direction of the incoming streams and crossflow as there is a 90° angle between the incoming flow direction and the flow inside the heat pipes. Both crossflow heat exchangers and counter-flow heat exchangers have a higher effectiveness than other heat exchanger geometries [14].

Faghri [11] and Jouhara [15, 16] provide a review on current applications for heat pipes and some examples include solar water heating [17, 18, 19, 20], desalination [21, 22] and domestic space heating applications [23, 24]. However, one of the most promising applications is in WHR. Existing WHR applications of HPHEs include: an EU project, ETEKINA [25], with installations of HPHE technology within steel, aluminium and ceramic industries [26]; the DREAM Project (Design for Resource and Energy efficiency in cerAMic kilns) with specific focus on the application of HPHEs to a kiln cooling section [27]; and i-ThERM, an EU funded project which looked at the development of an array of technology related to heat pipes and in particular to heat recovery focusing on energy transfer by the radiation mechanism [28]. An example of a 12.6 MW HPHE installed to recover energy contained within exhaust gas from a steel mill blast furnace is shown in Figure 3.



Figure 3: A functioning heat pipe heat exchanger unit.

2.2 Working Fluid

When choosing the working fluid inside the heat pipe, the main limits are the liquid boiling and vapour condensation temperatures of each fluid. Ref. [29] provides examples of available and tested working fluids with their applicable temperature ranges. Since the heat pipe is effectively working at a constant temperature, one must be aware of the range of boiling temperatures of different fluids as it is possible to boil all the working fluid in the heat pipe and reach the 'dry out' limit. Heat pipe design is outside the scope of this paper, but the choice of working fluid usually comes down to the working temperatures, and its effectiveness is measured by the specific heat of the fluid. For low grade heat recovery, distilled water is ideal due to its high specific heat [29].

For most applications the working fluid inside the heat pipe itself is assumed to be isothermal throughout the heat pipe's length. However, there is a small temperature difference which determines the figure of merit of the heat pipe. A figure of merit is a measure of the heat pipe's thermal resistance; a high figure of merit for the fluid in a thermosyphon means that the heat pipe will have a low temperature difference between its two ends. Consequently, a heat pipe with a high figure of merit can achieve a good performance due to its low thermal resistance and high heat transfer capability [30]. The figure of merit also depends on the operating temperature of the heat pipe. Equation (2-1) calculates figure of merit values for typical working fluids in thermosyphons:

$$\Phi = \left(\frac{h_{fg} k_l^3 \rho_l^2}{\mu_l} \right)^{1/4} \quad (2-1)$$

where Φ is the figure of merit ($\text{kg.K}^{-3/4}.\text{s}^{-5/2}$), h_{fg} is the latent heat of vaporisation (J.kg^{-1}), k_l is the thermal conductivity of the working fluid ($\text{W.m}^{-1}.\text{K}^{-1}$), ρ_l is the density of the working fluid (kg.m^{-3}) and μ_l is the liquid viscosity (Pa.s^{-1}) [31]. A visualisation of the application of this equation is shown in Figure 4.

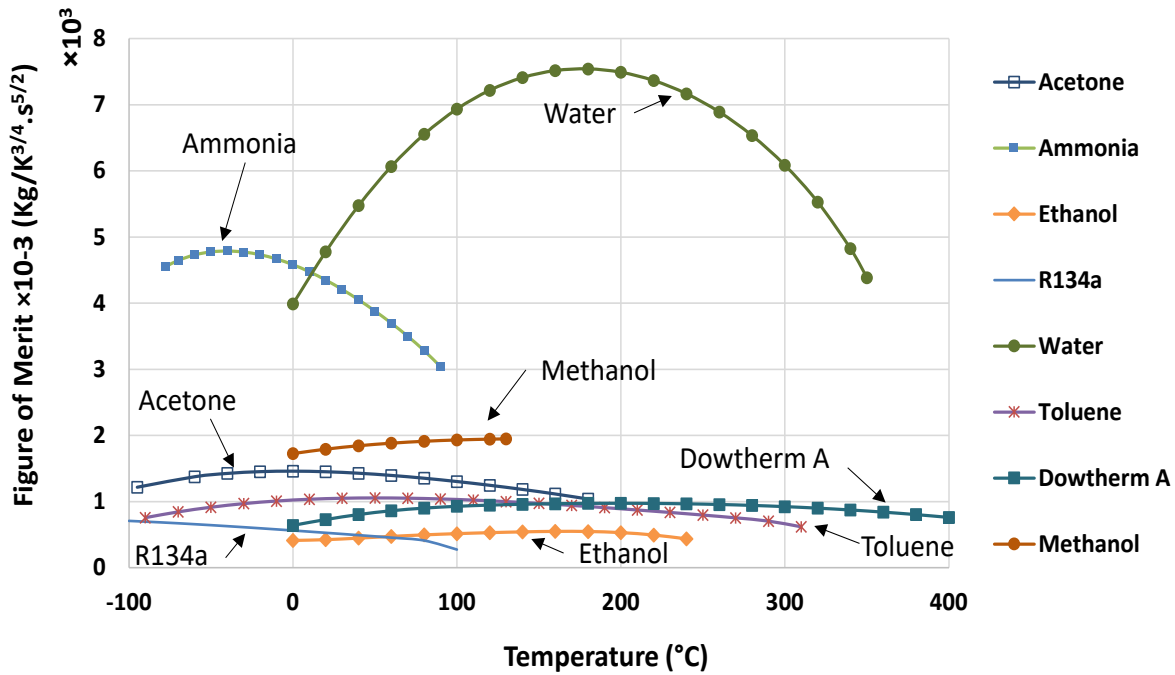


Figure 4: Figure of merit values for typical working fluids at a range of temperatures in a thermosyphon [32].

2.3 Transient Conditions and Previous Modelling

HPHEs tend to be installed in challenging streams and as such, each unit is bespoke for a specific plant's needs. In order to predict its size, numerous papers in literature have referenced using the Effectiveness-Number of Transfer Units (ϵ -NTU) method [33, 34, 35]. A limitation so far of this method is that it has only been applied to HPHEs operating under steady-state conditions or with averaged values, which are often the exception in real life heat recovery systems unless significant control measures are undertaken.

Regarding literature on modelling transient heat pipe behaviour, the first few mentions of models are the works by Chang and Colwell [36] who compared numerical predictions to experimental data and achieved a moderate level of success. Due to limited technology at the time, the computational model assumed that the dominant heat transfer modes were two-dimensional conduction in the heat pipe shell and wick. Other variables were neglected such as the thermal resistance along the vapour space and along the liquid-vapour interface. Performance was predicted using a finite-difference method.

Many of the first transient heat pipe models dealt with start-up problems, particularly the change of solid working fluids into liquid and eventually gas. For example, Deverall et al. [37]

described the transient behaviour of water and metallic heat pipes. They concluded that start-up was possible from a solid-state working fluid, however, it was highly dependent on the amount of heat provided.

Colwell [38] is one of the first published pieces of work that attempts to model the complete transient behaviour of a heat pipe. In his work he models a heat pipe with a metallic working fluid for high temperature applications, during start-up from a frozen state.

Another example of start-up from frozen state is from Yang et al. [39] who developed a transient analysis code for a flat heat pipe receiver in a solar power tower plant. The model was able to predict the temperature distributions reasonably well, and the experimental results showed promise for the application of flat heat pipes to solar towers.

Tournier and El-Genk developed their own two-dimensional heat pipe transient model [40], and the results achieved were in reasonable agreement with the experiments, albeit the transient response was found to be faster than in the experiment, due to the time taken for the heat to travel through the insulation. Brocheny [41] listed the state-of-the-art efforts on transient heat pipes and modelled the transient operation of low-temperature heat pipes from room-temperature conditions. He contributed to previous work by including dry-out and recovery in the thermal predictions. In terms of limitations, the effect of wick saturation was not considered in this work.

The earliest literature found regarding the use of TRNSYS and heat pipes was in 2003 by Budihardjo, Morrison and Behnia [42]. This work developed TRNSYS models for predicting the performance of water-in-glass evacuated tube solar water heaters (Figure 5). Though not WHR or a HPHE, this work highlighted the use of TRNSYS to simulate 21 inclined open thermosyphons. TRNSYS was used to simulate the collector efficiency and natural circulation flow rate.

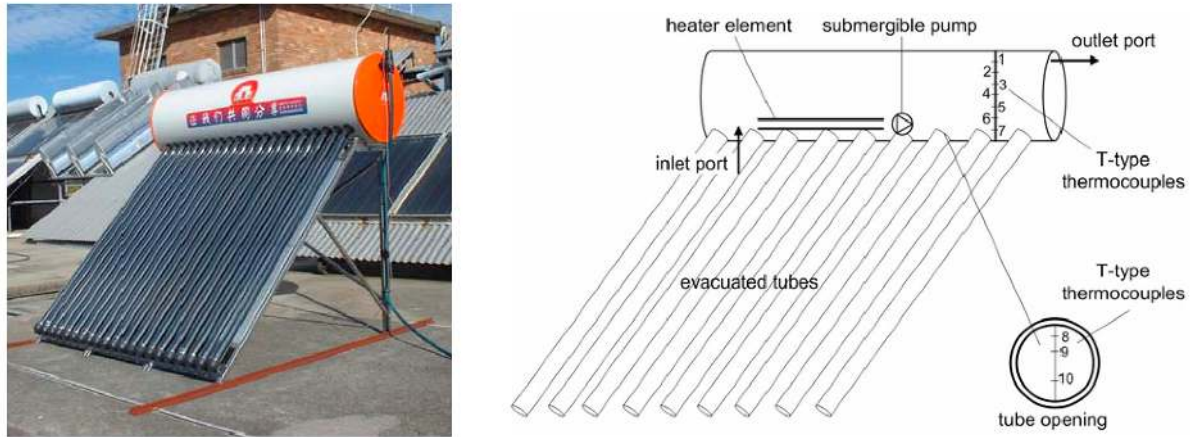


Figure 5: Schematic and photo of water-in-glass evacuated tube solar water heater [43].

Yau and Tucker [43] in the same year calculated the overall effectiveness of a wet six-row wickless HPHE for a HVAC system. The main aim was to determine whether moisture content and film condensation on fins reduced the total effectiveness value of the HPHE. This was a very small lab scale unit consisting of six copper heat pipes with an outer diameter of 9.55 mm and finned with 315 0.33mm aluminium fins per metre. The TRNSYS model for the HPHE is the closest work related to this presented work. The model simulates a lab scale HPHE for only copper heat pipes and fins to determine the overall effectiveness of this heat exchanger and specially requires an inclination angle and humidity of the air. This is an example of WHR but the focus of the work was on HVAC systems and removing humidity from air, particularly for hospitals, and predicting the onset of film condensation. This model used hour-by-hour climatic data from Kuala Lumpur and dealt with low temperature ranges i.e. $<35^{\circ}\text{C}$.

The HPHE component presented here can simulate multiple heat sink fluids, any design configuration and number of heat pipes and is configured for WHR rather than dehumidification.

In 2005, Shah [44] provided a report on TRNSYS models of four types of evacuated tubular collectors, two of importance including heat pipes, namely:

- Type 238- Heat pipe evacuated tubular collectors with curved fins.
- Type 239- Heat pipe evacuated tubular collectors with flat fins.

Previous work by [45] saw the use of TRNSYS to model a multi-pass HPHE applied to a lab scale ceramic kiln using exhaust gases to preheat water. The authors noted the necessity for a dedicated HPHE component to simulate the performance more accurately rather than a counter-flow heat exchanger component. Energy recovery rates were within $\pm 15\%$ with an uncertainty of $< 5.8\%$, though temperature prediction differences of up to around 35% were seen. The model could not be confidently used for simulation predictions and used averaged values of conductance taken from the experimental work. This paper presents work that builds upon the conclusions previously published, whilst demonstrating validity on a full-scale installation using a component that can be used to predict performance in the future.

To date there has been no publications for a dedicated transient simulation component of a HPHE configured for WHR on an industrial scale. The aim of this paper is to fill this gap in knowledge using TRNSYS.

3 Theoretical Background

The aim of this chapter is to describe current methods of characterising HPHE performance and the principles behind how the TRNSYS component was created.

3.1 Methods of Calculating and Characterising HPHE Performance

There are currently three predominant methods available for predicting or characterising the performance of a heat exchanger. These are the Log Mean Temperature Difference (LMTD) method, the ϵ -NTU method and, more specifically for HPHEs, the thermal network analysis method.

3.1.1 The Logarithmic Mean Temperature Difference Method

The LMTD method can be used to quantify HPHE performance when inlet and outlet temperatures are known. This method can be used for steady-state but cannot be applied to the TRNSYS model requiring a transient simulation. The LMTD method oversimplifies the model as averaged values need to be used, which does not reflect the real nature of energy intensive processes. Furthermore, this is not a predictive method as outlet temperatures must be known. This method can be used for HPHEs but relies on previously determined data for inlets and outlets of an existing unit and so it is less useful for predicting performance. For a crossflow heat exchanger, the equation is [13]:

$$\Delta T_{LM} = \frac{(T_{e,in} - T_{c,out}) - (T_{h,out} - T_{c,in})}{\ln\left(\frac{T_{h,in} - T_{c,out}}{T_{h,out} - T_{c,in}}\right)} \quad (3-1)$$

3.1.2 Thermal Network Analysis

The thermal network analysis is a proven way of viewing the thermal resistances in a heat exchanger [35]. As each heat pipe is an individual miniature heat exchanger, they are all assumed to be heat transfer devices working in parallel with one another within a larger heat exchanger assembly. In an electrical circuit, resistance blocks the transfer of current, in a thermal energy analogy, current is heat flow and resistance is thermal resistance (R), defined as the difference in temperature (ΔT) divided by the heat transfer rate (\dot{Q}), as shown in Equation (3-2). This is better visualised as a thermal circuit, as shown in Figure 6.

$$R = \frac{\Delta T}{\dot{Q}} \text{ (K.W}^{-1}\text{)} \quad (3-2)$$

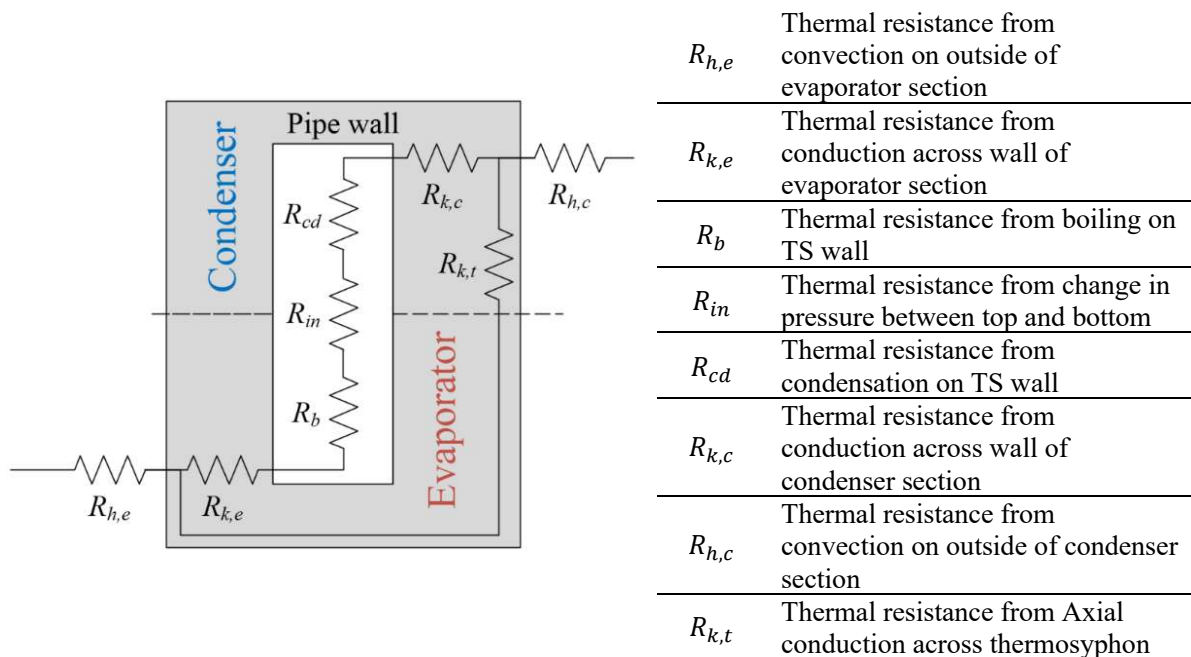


Figure 6: Schematic of the thermal resistances within a heat pipe [35].

This method is often used in tandem with the following ε -NTU method as the thermal resistances of the heat pipes are a requirement. Boiling [46], evaporation and condensation

correlations can also be used to calculate the resistances and heat transfer performance of thermosyphons [47].

3.1.3 The Effectiveness-NTU Method

The ε -NTU method is used to predict outlet temperatures by calculating the effectiveness, a dimensionless parameter related to the heat transfer performance of the heat exchanger. It is a measure between 0 and 1 and it is the measure of the actual heat transfer rate compared to the maximum theoretical heat transfer rate for the heat exchanger. This method was determined to be the most useful for transient predictions and was used to create the TRNSYS component. The general equation is shown below and has been developed for the evaporator and condenser sections of a HPHE [35]:

$$\varepsilon_e = \frac{q_{act}}{q_{max}} = \frac{C_e(T_{e,in} - T_{e,out})}{C_{min}(T_{e,in} - T_{c,in})} \text{ and } \varepsilon_c = \frac{C_c(T_{c,out} - T_{c,in})}{C_{min}(T_{e,in} - T_{c,in})} \quad (3-3)$$

3.2 Using the Effectiveness-NTU and Thermal Network Analysis Methods to Predict HPHE Performance.

To determine the equations requiring coding for the TRNSYS HPHE component, the ε -NTU equations needed to be expanded to their base components so that the relevant TRNSYS inputs, parameters and calculations could be fed into the equations. Equations (3-4) and (3-5) are developed from Equation (3-3), with ε_e and ε_c being the effectiveness of the evaporator and condenser sections. They show how the outlet temperatures for the evaporator and condenser section can be found from the effectiveness of that section.

$$T_{e,out} = T_{e,in} - \varepsilon_t \frac{C_{min}}{C_e} (T_{e,in} - T_{c,in}) \quad (3-4)$$

$$T_{c,out} = T_{c,in} + \varepsilon_t \frac{C_{min}}{C_c} (T_{e,in} - T_{c,in}) \quad (3-5)$$

where $T_{e,in}$, $T_{e,out}$, $T_{c,in}$ and $T_{c,out}$ are the inlet and outlet temperatures of the evaporator (e) and condenser (c) fluids, C_{min} is the minimum value of C_e and C_c , the heat capacities of the evaporator and condenser fluids, a measure of the mass flow rate (\dot{m} in $\text{kg}\cdot\text{s}^{-1}$) multiplied by the specific heat capacity (c_p in $\text{J}\cdot\text{kg}^{-1}\cdot\text{K}^{-1}$) of each stream. ε_t is the total effectiveness of the

heat exchanger, traditionally calculated using the equations below, Depending on which heat capacity is the larger of the condenser and evaporator fluids, the total effectiveness (ε_t) equation varies:

$$\text{If } C_e > C_c \quad \varepsilon_t = \left(\frac{1}{\varepsilon_{c,n}} + \frac{C_c/C_e}{\varepsilon_{e,n}} \right)^{-1} \quad (3-6)$$

$$\text{If } C_c > C_e \quad \varepsilon_t = \left(\frac{1}{\varepsilon_{e,n}} + \frac{C_e/C_c}{\varepsilon_{c,n}} \right)^{-1} \quad (3-7)$$

where $\varepsilon_{c,n}$ and $\varepsilon_{e,n}$ are the effectiveness associated with a transverse row of thermosyphons. For this reason, different equations are coded into the component depending on whether C_e or C_c is larger. The effectiveness of a row of evaporator ($\varepsilon_{e,n}$) or condenser ($\varepsilon_{c,n}$) thermosyphons can be written by Equations (3-8) and (3-9), respectively.

$$\varepsilon_{e,n} = 1 - (1 - \varepsilon_e)^{N_t} \quad (3-8)$$

$$\varepsilon_{c,n} = 1 - (1 - \varepsilon_c)^{N_t} \quad (3-9)$$

where ε_e and ε_c are the effectiveness of a single thermosyphon's evaporator or condenser section and N_t is the number of thermosyphons in a row. The effectiveness of the evaporator and condenser sections of a thermosyphon can be written by Equations (3-10) and (3-11).

$$\varepsilon_e = 1 - e^{(-NTU_e)} \quad (3-10)$$

$$\varepsilon_c = 1 - e^{(-NTU_c)} \quad (3-11)$$

where NTU_e and NTU_c are the number of transfer units for the evaporator and condenser. The number of transfer units of the evaporator and condenser sections (NTU_e and NTU_c) are equivalent to Equations (3-12) and (3-13).

$$NTU_e \equiv \frac{U_e A_e}{C_e} \quad (3-12)$$

$$NTU_c \equiv \frac{U_c A_c}{C_c} \quad (3-13)$$

where U_e and U_c are the overall heat transfer coefficients of the evaporator and condenser section of the thermosyphon and A_e and A_c are the overall heat transfer areas.

With a HPHE, the UA values are equivalent to the inverse of the thermal resistance of that section and U is equal to h_{fc} , the forced convection heat transfer coefficient. This is shown in Equations (3-14) and (3-15):

$$U_e A_e = \frac{1}{R_{e,out}} = h_{fc,e} A_e \quad (3-14)$$

$$U_c A_c = \frac{1}{R_{c,out}} = h_{fc,c} A_c \quad (3-15)$$

where $R_{e,out}$ and $R_{c,out}$ are the thermal resistances of the evaporator section and the condenser section. The thermal resistance decreases as the number of pipes increases, due to the increased surface area. Section 3.3 deals with how h_{fc} is calculated.

Heat capacitance is found by Equations (3-16) and (3-17).

$$C_e = \dot{m}_e c_{p,e} \quad (3-16)$$

$$C_c = \dot{m}_c c_{p,c} \quad (3-17)$$

where \dot{m}_e and \dot{m}_c are the mass flow rates of the evaporator and condenser streams and $c_{p,e}$ and $c_{p,c}$ are the specific heat capacities of the fluids.

The equations in this section, along with others, were coded using Fortran language for the HPHE component in the TRNSYS model to determine the outlet temperatures depending on the variables in the model.

3.3 Calculating the Heat Transfer Coefficient of Forced Convection

The heat transfer coefficient of forced convection, h_{fc} , is the most challenging variable to determine and it depends on a variety of flow properties. The calculations predominantly depend upon the design of the HPHE. h_{fc} must be calculated for both the evaporator and condenser sections, as below:

$$h_{fc} = \frac{Nu_D \times k}{D_o} \quad (3-18)$$

Nu_D is the Nusselt number (dimensionless) in respect to the diameter of the heat pipe and the calculations are shown in Section 3.3.1, k is the thermal conductivity of the fluid ($\text{W}\cdot\text{m}^{-1}\cdot\text{K}^{-1}$) and D_o is the outer diameter of the heat pipe (m).

3.3.1 Nusselt, Prandtl and Reynolds Dimensionless Numbers

Each of the numbers below are calculated for the inlet, outlet and heat pipe outer wall temperatures of both the evaporator and condenser sections. Tables for natural gas, flue gas, air, water and thermal oil (specifically Therminol-66) are used to calculate the thermophysical properties from [48, 49, 50, 51]. The significant properties are density, kinematic viscosity, thermal conductivity and specific heat capacity.

The Nusselt number is traditionally calculated from Equation (3-19), a rearrangement of Equation (3-18) in order to create a non-dimensional number from many contributing variables. In essence, the Nusselt number represents a ratio of heat transfer by convection to conduction across a fluid layer to quantify which mechanism contributes the most to heat transfer [13].

$$Nu = \frac{hL_{ch}}{k} \quad (3-19)$$

L_{ch} is the characteristic length, in this case substituted with D_o .

The Prandtl number (Pr) of a fluid is the ratio between momentum diffusivity and thermal diffusivity. The number describes the thickness of the thermal boundary layer relative to the thermal boundary layer. Gases have Prandtl numbers around 0.7-1.0 and water is 1.7-13.7. [13]. The Prandtl number can be calculated from Equation (3-20) [52].

$$Pr = \frac{\text{Momentum diffusivity of momentum}}{\text{Thermal diffusivity of heat}} = \frac{\nu}{\alpha} = \frac{\mu/\rho}{k/c_p\rho} = \frac{c_p\mu}{k} \quad (3-20)$$

ν is the momentum or kinematic viscosity ($\text{m}^2.\text{s}^{-1}$), α is the thermal diffusivity ($\text{m}^2.\text{s}^{-1}$), μ is the dynamic viscosity (Pa.s), ρ is the density (kg.m^{-3}), k is the thermal conductivity ($\text{W.m}^{-1}.\text{K}^{-1}$), c_p is the specific heat ($\text{J.kg}^{-1}.\text{K}^{-1}$).

The Reynolds number (Re) provides an indication of the flow regime and also when laminar flow will transition to turbulent flow. Large Reynolds number indicate turbulent flow and a quick transition and *vice versa* for a small Reynolds number. [13]. Figure 7 shows typical Reynolds numbers associated with crossflow flow patterns and Equation (3-21) the general equation used to determine the Reynolds number.

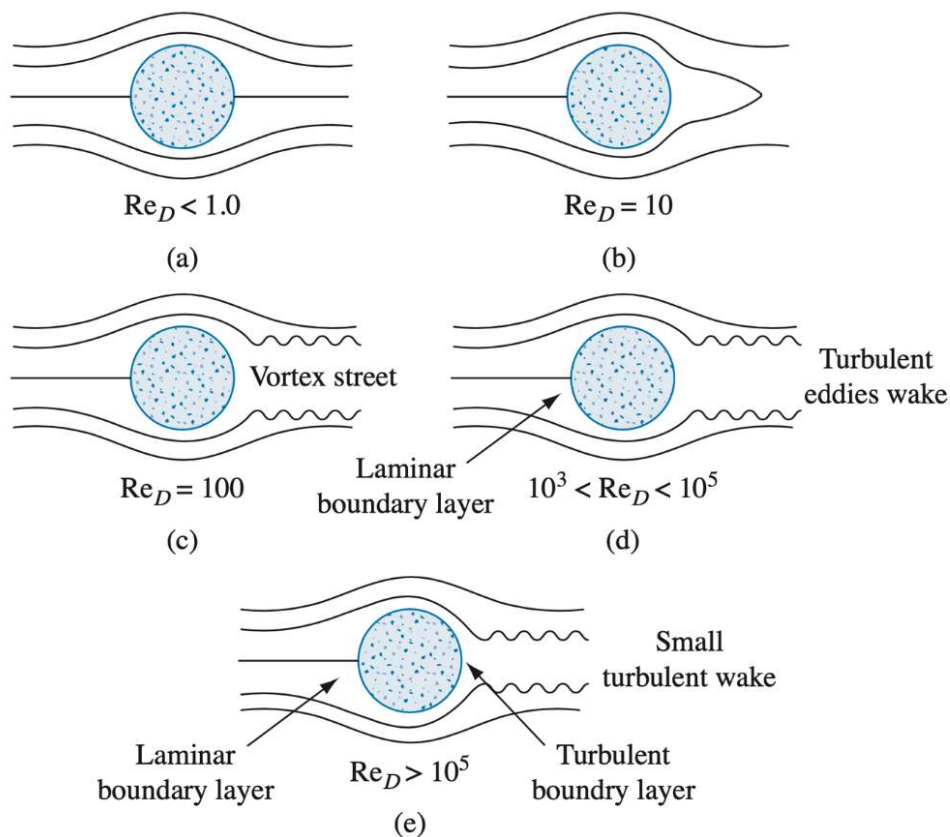


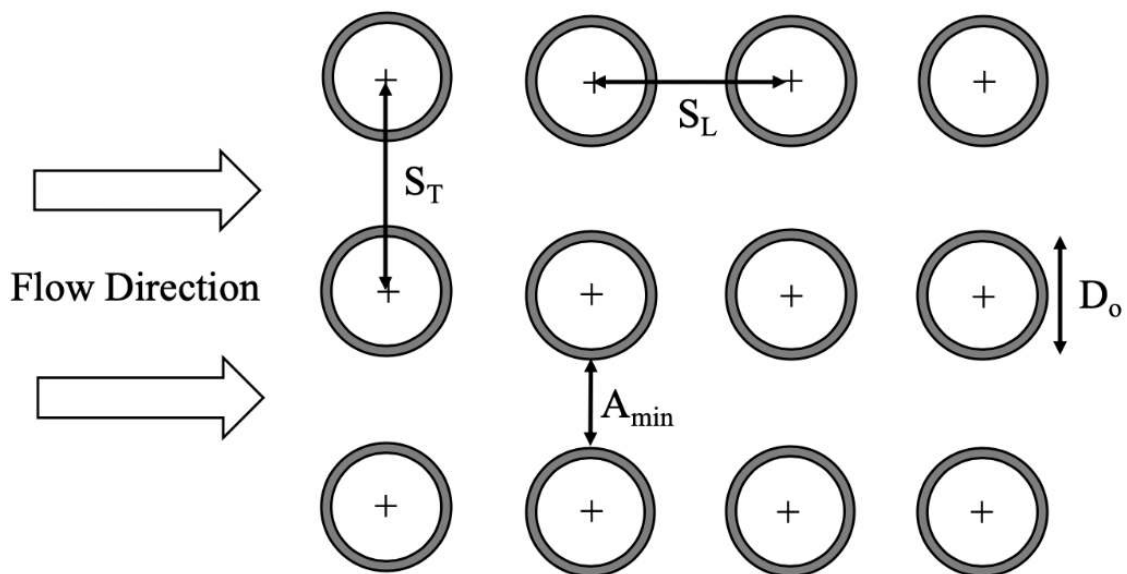
Figure 7: Crossflow flow patterns for fluids passing across a cylinder with increasing Reynolds number [53].

$$Re = \frac{\text{Inertial forces}}{\text{Viscous forces}} = \frac{\rho u L_{ch}}{\mu} = \frac{u L_{ch}}{\nu} \quad (3-21)$$

where ρ is the fluid density, u is the velocity, μ is the dynamic viscosity, L_{ch} is the characteristic length and ν is the momentum or kinematic viscosity. The Reynolds number associated with the outer diameter of a tube (D_o) can be determined using:

$$Re_D = \frac{V_{max} D_o}{\nu} \quad (3-22)$$

The calculation of V_{max} , the maximum velocity occurring in the minimum flow area between tubes (in this case the heat pipes), depends on whether the tubes are in a staggered or in-line arrangement. Figure 8 shows an in-line tube bundle arrangement with the varying parameters and Equation (3-24) provides the calculation. Figure 9 shows a staggered arrangement with the V_{max} calculations provided by Equations (3-25) to (3-27).



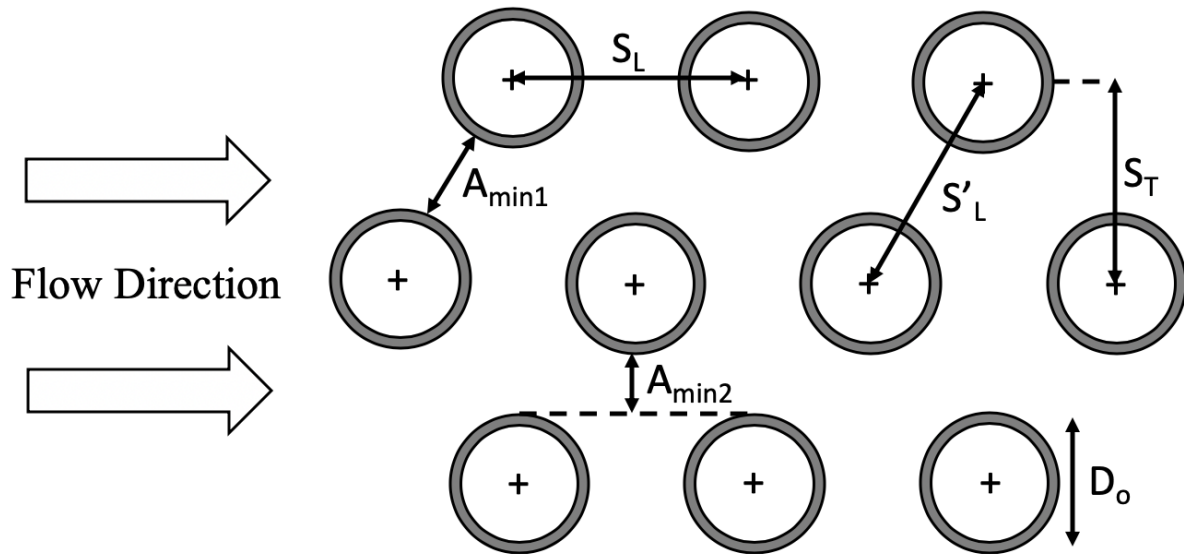
- S_T - Transverse row pitch
- S_L - Longitudinal row pitch
- D_o - Outer diameter
- A_{min} - Location of minimum free area

Figure 8: In-line tube bundle arrangement.

$$A_{min} = S_T - D_o \quad (3-23)$$

$$V_{max} = \frac{S_T}{S_T - D_o} \times v_f \quad (3-24)$$

where v_f is the free-flow velocity at the inlet face area without tubes.



- S_T - Transverse row pitch
- S_L - Longitudinal row pitch
- S'_L - Diagonal distance between longitudinal centres
- D_o - Outer diameter
- $A_{min1/2}$ - Potential locations of minimum cross flow area

Figure 9: Staggered tube bundle arrangement.

The minimum free-flow area, A_{min} , can potentially occur in two places in staggered arrangements. It can be, as in Equation (3-23), transversely between the tube rows. However, if S_T is much larger than S_L such that:

$$\sqrt{\left(\frac{S_T}{2}\right)^2 + S_L^2} < \frac{S_T + D_o}{2} \quad (3-25)$$

according to [53]:

$$V_{max} = \frac{S_T/2}{\sqrt{\left(\frac{S_T}{2}\right)^2 + S_L^2 - D_o}} \times v_f \quad (3-26)$$

The authors have rearranged this to:

$$V_{max} = \frac{v_f}{\sqrt{1 + \left(2\frac{S_L}{S_T}\right)^2 - 2\frac{D_o}{S_T}}} \quad (3-27)$$

Table 1 provides the available correlations, based on empirical data, for calculating the Nusselt number from literature using Reynolds and Prandtl numbers with the varying applications and conditions where they can be applied; adapted from [54].

Table 1: Available correlations for calculation Nusselt numbers over tube bundles.

| Ref. | Equation | Condition | Equation |
|------|--|---|----------|
| [55] | $Nu_D = 0.33Re_D^{0.6}Pr^{1/3}$ | Staggered >10 rows $10 < Re_D < 40,000$ | (3-28) |
| [56] | $Nu_D = KRe_D^n$ K and n values are tabulated in [57, 53] | Air only >10 rows | (3-29) |
| [14] | $Nu_D = K_1Re_D^n$ K_1 and n values are tabulated in [57, 53] | Air only <10 rows | (3-30) |
| [56] | $Nu_D = 0.32F_aRe_D^{0.61}Pr^{0.31}$ F_a is an arrangement correction factor provided in [56] | | (3-31) |
| [58] | $Nu_D = 0.34F_aRe_D^{0.61}Pr^{0.31}$ $F_a = 1 + \left(S_L + \frac{7.17}{S_L} - 6.52\right) \times \left[\frac{0.266}{(S_T - 0.8)^2} - 0.12\right]$ $\times \sqrt{\frac{1000}{Re_D}}$ | In-line | (3-32) |
| | $Nu_D = 0.35F_aRe_D^{0.57}Pr^{0.31}$ | Staggered | (3-33) |

| | | | |
|------|--|--|---------------|
| | $F_a = 1 + \frac{S_L}{10} + \frac{0.34}{S_T}$ | | |
| [59] | $Nu_D = 0.9Re_D^{0.4}Pr^{0.36}(Pr/Pr_s)^{0.25}$ | >16 rows 0-100 Re_D In-line | (3-34) |
| | $Nu_D = 0.52Re_D^{0.5}Pr^{0.36}(Pr/Pr_s)^{0.25}$ | >16 rows 100-1000 Re_D In-line | (3-35) |
| | $Nu_D = 0.27Re_D^{0.63}Pr^{0.36}(Pr/Pr_s)^{0.25}$ | >16 rows 1000-20,000 Re_D In-line | (3-36) |
| | $Nu_D = 0.033Re_D^{0.8}Pr^{0.4}(Pr/Pr_s)^{0.25}$ | >16 rows 20,000-200,000 Re_D In-line | (3-37) |
| | $Nu_D = 1.04Re_D^{0.4}Pr^{0.36}(Pr/Pr_s)^{0.25}$ | >16 rows 0-500 Re_D Staggered | (3-38) |
| | $Nu_D = 0.71Re_D^{0.5}Pr^{0.36}(Pr/Pr_s)^{0.25}$ | >16 rows 500-1000 Re_D Staggered | (3-39) |
| | $Nu_D = 0.35(S_T/S_L)^{0.2}Re_D^{0.6}Pr^{0.36}(Pr/Pr_s)^{0.25}$ | >16 rows 1000-20,000 Re_D Staggered | (3-40) |
| | $Nu_D = 0.031(S_T/S_L)^{0.2}Re_D^{0.8}Pr^{0.36}(Pr/Pr_s)^{0.25}$ | >16 rows 20,000-200,000 Re_D Staggered | (3-41) |
| [53] | $Nu_D = 0.8Re_D^{0.4}Pr^{0.36}(Pr/Pr_s)^{0.25}$ | >10 rows 0.7<Pr<500 10< Re_D <100 In-line | (3-42) |
| | $Nu_D = 0.9Re_D^{0.4}Pr^{0.36}(Pr/Pr_s)^{0.25}$ | >10 rows 0.7<Pr<500 10< Re_D <100 | (3-43) |

| | | | |
|--|--|---|---------------|
| | | Staggered | |
| | $Nu_D = 0.27Re_D^{0.63}Pr^{0.36}(Pr/Pr_s)^{0.25}$ | 0.7<Pr<500 1000<Re _D <10,000 In line S _T /S _L ≥0.7 | (3-44) |
| | $Nu_D = 0.35\left(\frac{S_T}{S_L}\right)^{0.2}Re_D^{0.6}Pr^{0.36}(Pr/Pr_s)^{0.25}$ | 0.7<Pr<500 1000<Re _D <10,000 Staggered S _T /S _L <2 | (3-45) |
| | $Nu_D = 0.4Re_D^{0.6}Pr^{0.36}(Pr/Pr_s)^{0.25}$ | 0.7<Pr<500 1000<Re _D <10,000 Staggered S _T /S _L ≥2 | (3-46) |
| | $Nu_D = 0.021Re_D^{0.84}Pr^{0.36}(Pr/Pr_s)^{0.25}$ | 0.7<Pr<500 Re _D >10,000 In-line | (3-47) |
| | $Nu_D = 0.022Re_D^{0.84}Pr^{0.36}(Pr/Pr_s)^{0.25}$ | 0.7<Pr<500 Re _D >10,000 Staggered | (3-48) |
| | $Nu_D = 0.019Re_D^{0.84}$ | Pr=0.7 Re _D >10,000 Staggered | (3-49) |
| | $Nu_D = 0.0131Re_D^{0.883}Pr^{0.36}$ | 450,000<Re _D <700,000 Staggered S _T /D=2 S _L /D=1.4 | (3-50) |

Pr_s is the Prandtl number evaluated at the external wall temperature of the heat pipe.

For the correlations provided by Ref. [59], if the number of rows (Nr) is <16 and Re_D >1000, a correction factor can be used as seen in Table 2, adapted from [13].

Table 2: Correction Factor for Zukauskas Correlations with <16 Rows of Heat Pipes [13].

| <i>Nr</i> | 1 | 2 | 3 | 4 | 5 | 7 | 10 | 13 |
|-----------|------|------|------|------|------|------|------|------|
| In-line | 0.70 | 0.80 | 0.86 | 0.90 | 0.93 | 0.96 | 0.98 | 0.99 |
| Staggered | 0.64 | 0.76 | 0.84 | 0.89 | | | | |

3.3.2 Effect of Finning Heat Pipes

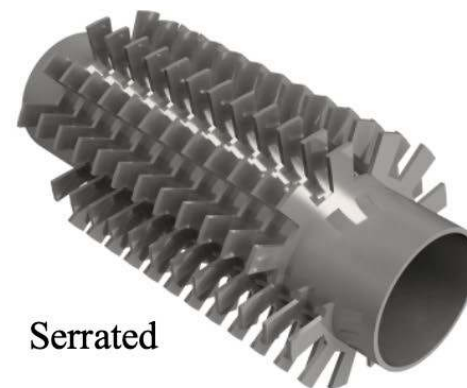
The final factor that needs to be considered is whether the heat pipes are finned. External pipe finning is used to increase the heat transfer surface and increase turbulence and is primarily for gaseous applications but can also be used for liquids. The HPHE tested had helical fins on both the evaporator and condenser sections. Helical fins are currently the favoured configuration for heat exchangers for WHR units. Ponsoi, Pikulkajorn and Wongwises [60] provide a thorough review on spiral finning, the available configurations and available correlations for Colburn and friction factors. Figure 10 provides a schematic of a selection of available tube finning configurations. The model can be adapted to incorporate other finning configurations and used equations for their area and correlations determining efficiency.



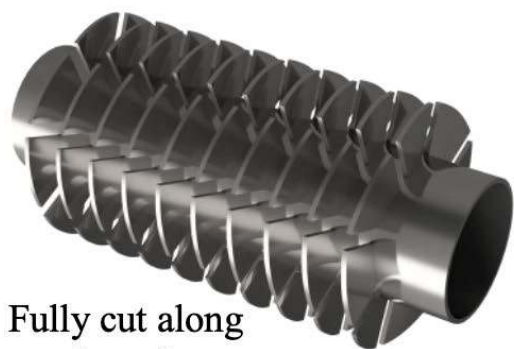
Annular



Helical



Serrated



Fully cut along
the axis



Fully cut
on helix



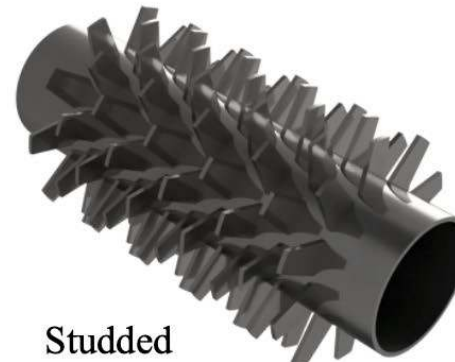
Partially cut
on helix



Slotted
helical



Slotted wavy
helical



Studded

Figure 10: A selection of available fin configurations.

The total heat transfer area (A_{tot}) of a heat pipe section with fins is found by adding the heat transfer area of the heat pipe (A_{hp}) to the heat transfer area of the fins (A_f) taking into account the efficiency of the fins. Heat transfer is reduced the farther the fin section is from the pipe as the energy is passed by conduction. Therefore, a coefficient of efficiency for the fin is introduced (η_f). Figure 11 shows a diagram of a finned heat pipe and symbols used in the following equations. These equations are calculated for both the evaporator and condenser section separately for helical fins.

$$A_{tot} = A_{hp} + \eta_f A_f \quad (3-51)$$

$$\eta_f = \frac{\tanh(xH_f)}{xH_f} \quad (3-52)$$

H_f is the width of the fins and x is:

$$x = \sqrt{\frac{2h_{fc}}{k_f e_f}} \quad (3-53)$$

h_{fc} is the heat transfer coefficient of forced convection, k_f is the thermal conductivity of the fin material, e_f is the thickness of the fin.

The heat transfer area of the fins is:

$$A_f = 2\pi H_f L_{hl} N_t \quad (3-54)$$

L_{hl} is the length of the helical found by:

$$L_{hl} = \frac{L}{P_f} \sqrt{\left(\pi \frac{D_{of} + D_o}{2}\right)^2 + P_f^2} \quad (3-55)$$

L is the length of the finned heat pipe section, whether it is the evaporator or condenser. D_{of} is the outer diameter of the heat pipe including the fins, D_o is the outer diameter of the heat pipe and P_f is the pitch of the fins.

The heat transfer area of just the heat pipe (A_{hp}) without fins is found by:

$$A_{hp} = \pi D_o L \quad (3-56)$$

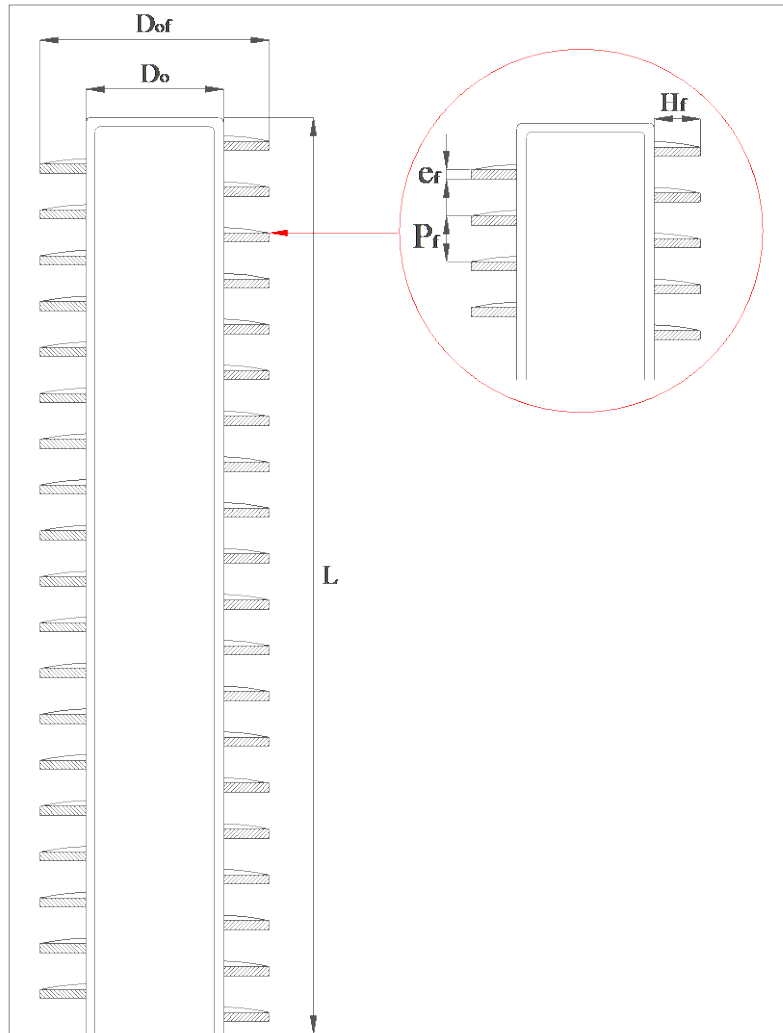


Figure 11: Diagram of helical finning with symbols.

A HPHE consists of many individual heat pipes. The heat transfer area in the entire exchanger condenser A_c and evaporator A_e section is determined by:

$$A_c = N_r N_t A_{tot,c} \quad (3-57)$$

$$A_e = N_r N_t A_{tot,e} \quad (3-58)$$

3.3.2.1 Thermal conductivity of carbon steel fins

As well as the fin configuration, the thermal conductivity of the material type of fins used in heat exchangers is vital to the overall fin efficiency. The fin material in the HPHE unit used to validate the model was carbon steel. The thermal conductivity of the fins, k_f , was determined using data from [61]. This was extracted to create Figure 12. Carbon steel is predominantly used for finning but the use of aluminium or forms of stainless steel is also seen. The model can be altered to use other material thermal conductivity characteristics, if required.

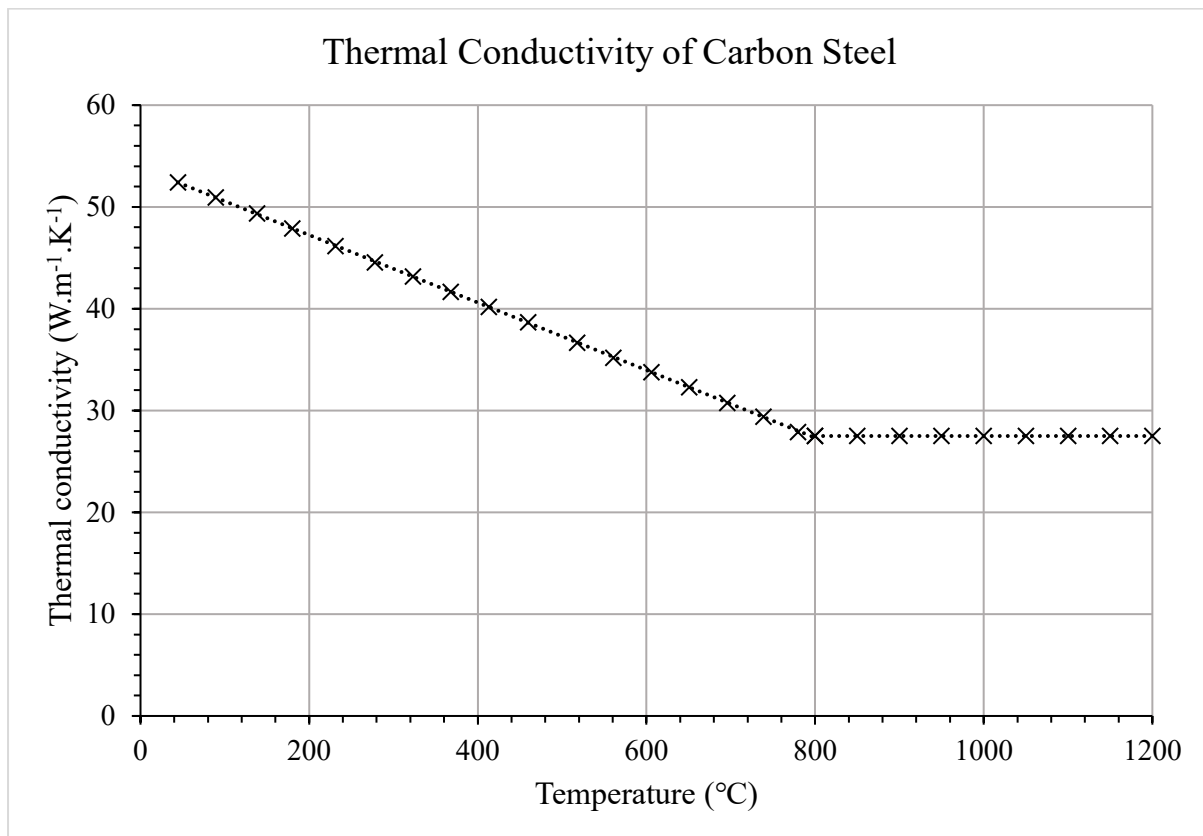


Figure 12: Thermal conductivity of carbon steel [61].

4 Methodology

A desktop simulation has been conducted with a personally developed transient HPHE model and results compared with experimental data. The software TRNSYS (TRaNsient System Simulation) 17 was used to create a transient simulation with varying inputs and parameters. This simulation engine was developed by members of the Solar Energy Laboratory at the College of Engineering within the University of Wisconsin. The software is used to study thermal systems and has latterly been employed to study waste heat recovery. It is installed

with a library of over 150 components. These components are used to model a transient system, which allows the user to evaluate and analyse chosen inputs and parameters and view results. An interface called 'Simulation Studio' is used where the system is graphically modelled using the library of components, which are known as 'Types'. These Types are internally composed of a series of mathematical equations where inputs and parameters are converted to output values. The values and units of the inputs and parameters can be altered to provide a graphical view of the system's functionality over a set period of time. A parameter is fixed throughout the entire simulation, but an input can be fixed or changed in each iteration step over the simulation. A transient nature can be achieved by linking an external file (.txt/.csv) as the input or linking the output of another component as the input for another, for example, data logged real temperature profiles from a furnace or weather temperature data from cities around the world can be used.

A HPHE component is not available in the TRNSYS library and so the authors coded a new component. The standard TRNSYS library with the location of the newly created HPHE Type is shown in Figure 13. The component needs a 'skeleton' where the user can change inputs and

parameters, which is also the icon that can be visualised in simulation studio. It then has the internal mathematical operation which takes the inputs and creates the outputs.

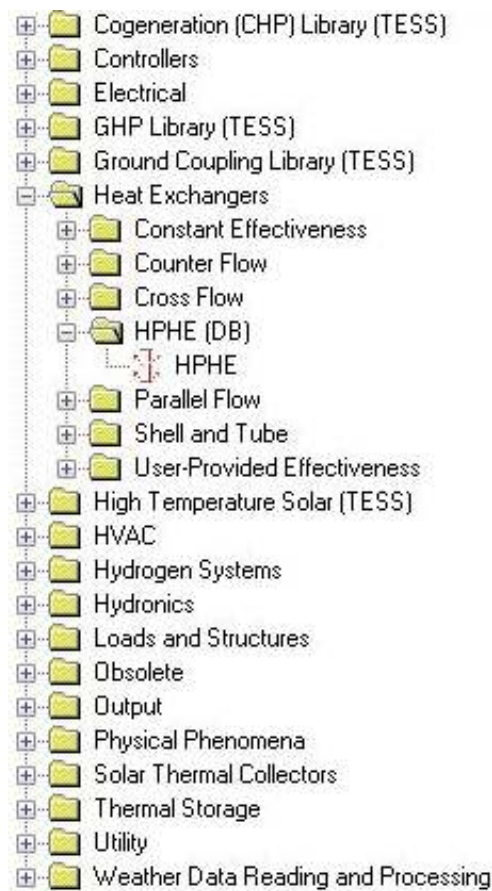


Figure 13: A view of the standard TRNSYS component library and the location of the newly developed HPHE component.

4.1 Process for Coding the HPHE Component

The process for coding and including a new component in the TRNSYS library is not straightforward; it requires the use of multiple software and is coded in Fortran. Fortran (FORmula TRANslation) is a compiled imperative programming language. TRNSYS was written in this language and as such, it is required to code a Type in this language and then compile it. The Fortran language was developed by the International Business Machines (IBM) Corporation in the 1950s for the purpose of numerical computation and scientific computing specifically for engineering and scientific purposes. The first manual was released in 1956 and the first compiler was released in 1957. The idea was to ease the process of inputting equations into computers. Fortran has many iterations and releases, specifically the Fortran 90 language was used to code the Type, developed in 1991. The process for creating a new component is

described in the Programmer’s guide (Volume 7) [62] provided within the software. However, not all sections or code is required so the process for building the novel HPHE Type is described in this section. Figure 14 provides a flowchart diagram to explain the coding process.

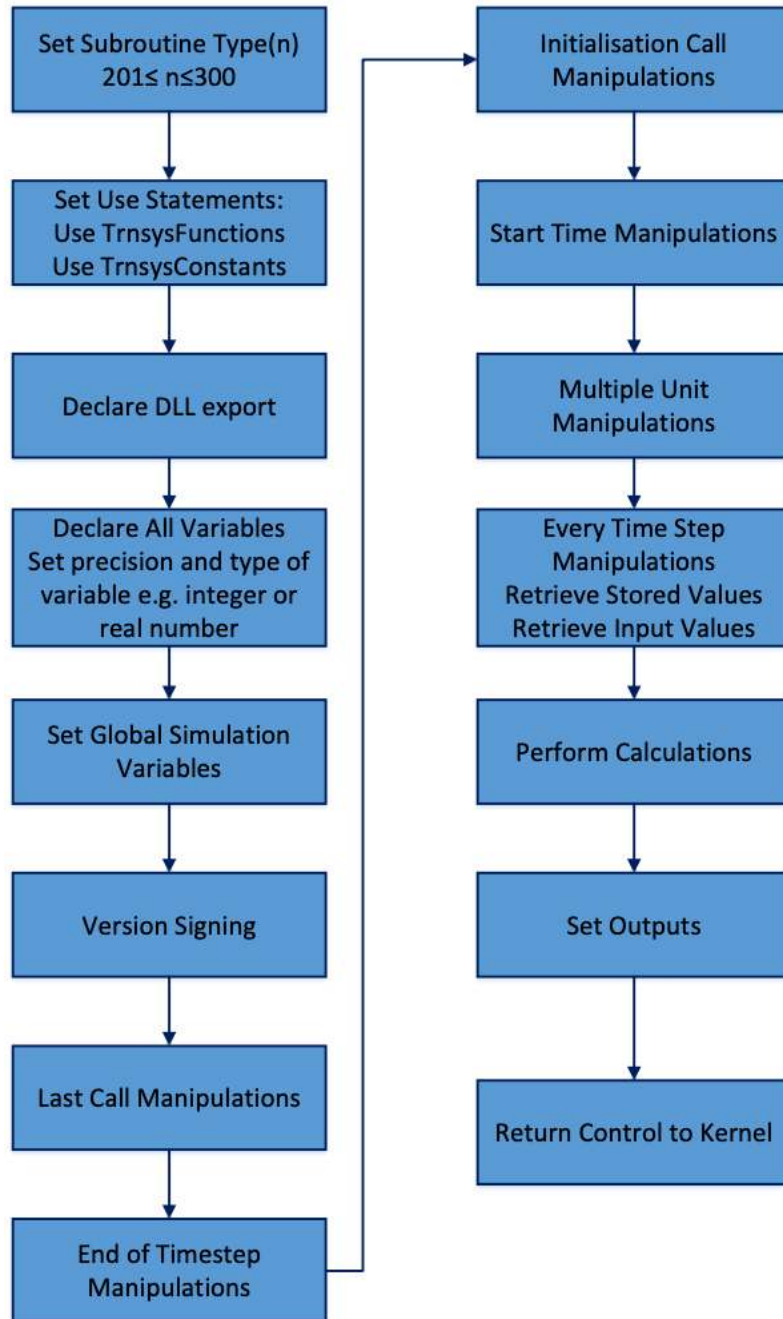


Figure 14: A flowchart of the TRNSYS component coding process.

To build a new model, TRNSYS 17 must be installed and a Fortran compiler capable of generating a 32-bit dynamic link library (DLL). Many compilers are available, but in this case

Intel Parallel Studio XE 2019 with the additional Intel Visual Fortran package was used. Intel Visual Fortran is an add-on for Microsoft Visual Basic.

The TRNSYS code is split into the kernel and the Types. The kernel provides all the background and functionality inputs to the Types. Types have the mathematical coding to perform calculations of the components used in the simulation as well as how to communicate with the kernel and call various other codes at given steps, in essence, converting inputs to outputs. Types distinguish between inputs that change with time and inputs that do not change with time. These are known as inputs and parameters, respectively. For the HPHE component, the following inputs were required, shown in Table 3.

Table 3: Inputs for HPHE TRNSYS component.

| Input | Designated Symbol | Units |
|------------------------------------|--------------------------|--------------------|
| Source fluid inlet temperature | Thi | °C |
| Sink fluid inlet temperature | Tci | °C |
| Mass flow rate of evaporator fluid | FLWe | kg.s ⁻¹ |
| Mass flow rate of condenser fluid | FLWc | kg.s ⁻¹ |

For the HPHE component, the following parameters were required, shown in Table 4.

Table 4: Parameters for HPHE TRNSYS component.

| Parameter | Designated Symbol | Units |
|---|--------------------------|----------------|
| Number of heat exchanger rows | Nr | N/A |
| Outer diameter of heat pipes | Dout | m |
| Length of active evaporator section | Le | m |
| Length of active condenser section | Lc | m |
| Number of heat pipes in row | Nt | N/A |
| Distance between heat centres in row | ST | m |
| Distance between heat pipe centres between rows | SL | m |
| Flow area of evaporator | Ae | m ² |
| Flow area of condenser | Ac | m ² |

| | | |
|------------------------|-------------|---|
| Finning Mode | FinningMode | - |
| Fluid Mode | FluidMode | - |
| Outer diameter of fins | Dofin | m |
| Thickness of fins | efin | m |
| Pitch of fins | Pfin | m |
| Width of fins | Hfin | m |

Within the Type, further internal calculations were carried out. These are summarised in the theoretical section of the paper.

4.1.1 HPHE Coding in Intel Visual Fortran

This section explains how the HPHE component (Type202) code was written. The first line of the code calls the particular subroutine to which the component in simulation studio is linked, in this case the Type number. Type numbers 201-300 are reserved for user written components and Type1-200 are reserved for the standard TRNSYS library. For this reason, Type202 was arbitrarily chosen.

A TRNSYS 17 simulation requires the access global constants and functions provided in the source code. To choose which are called into the simulation is done by ‘Use’ statements. Type202 requires *TrnsysConstants* and *TrnsysFunctions*. *TrnsysConstants* is a module containing fixed values that do not change throughout a simulation, for example, declaring the maximum amount of equations or outputs that can be used in a simulation. A table of these constants can be found in Section 7.4.1.1 of the Programmers manual [62]. *TrnsysFunctions* are all the functions that the subroutines can use to handle the stored data. A full description of each function is found in Section 7.4.2 of the Programmers manual [62].

In previous versions of TRNSYS, Types could not exist in an external *.dll file, it required altering the standard TRNDLL.dll. In TRNSYS 17, the Types can exist in an external *.dll. The kernel examines the contents of a user library directory to determine if any external *.dll files need to be loaded into the simulation. In this case, the Type202.dll file is an external *.dll file placed in the user library and is loaded into the memory for the duration of the simulation. The code below tells the kernel to search for Type202 in the user library and load it into the memory.

Declaring the variables is a section of code that comes after initially defining the subroutine, giving access to global variables and exporting the component. This is a larger section of code where all the local variables used through the simulation are given. *Implicit None* is used to instruct that all variables need to be explicitly declared. If the variable is a real number, *Double precision* is used to set the variable to be a real number with twice the amount of significant decimal digits and a magnitude range of 10^{-308} to 10^{308} . This accuracy is not necessary but modern computing power allows the use of it. *Integer* is used to set the variable to be an integer number. *Data* can be used before the variable to set a parameter to a fixed value; however, this command was not used for Type202. Figure 15 shows all the local variables used within the Type.

```

!Inputs
Double precision Thi !Temperature of source inlet fluid [deg C]
Double precision Tci !Temperature of sink inlet fluid [deg C]
Double precision FLWe !Mass flow rate evaporator (source) fluid [kg/s]
Double precision FLWc !Mass flow rate condenser (sink) fluid [kg/s]

!Parameters
Integer Nr !Number of rows in heat exchanger (longitudinal)
Double precision Dout !Outer diameter of heat pipes [m]
Double precision Le !Length evaporator [m]
Double precision Lc !Length of condenser [m]
Integer Nt !Number of tubes in row (transverse)
Double precision ST !Distance between row centres [m]
Double precision SL !Distance between heat pipe centres [m]
Double precision Ae !Flow area of evaporator [m2]
Double precision Ac !Flow area of condenser [m2]
Integer FinningMode !(1=none, 2=con finned, 3=evap finned, 4=both)
Integer FluidMode !Sink: 1=air 2=water 3=thermal oil
Double precision Dofin !Outer diameter of fins [m]
Double precision efin !Thickness of fins [m]
Double precision Pfin !Pitch of fins [m]
Double precision Hfin !Width of fins [m]

```

```

!Internal Variables
Double precision HTFe !Heat transfer coefficient evaporator [W/m2.K]
Double precision HTFeo !Heat transfer coefficient evaporator outlet [W/m2.K]
Double precision HTFc !Heat transfer coefficient condenser [W/m2.K]
Double precision HTFco !Heat transfer coefficient condenser outlet [W/m2.K]
Double precision HTAe !Heat transfer area of one evaporator row [m2]
Double precision HTAe_smooth !Heat transfer area of one evaporator row smooth [m2]
Double precision HTAc !Heat transfer area of one condenser row [m2]
Double precision HTAc_smooth !Heat transfer area of one condenser row smooth [m2]
Double precision Ce !Heat capacity rate of evaporator [j/K.s]
Double precision Ceo !Heat capacity rate of evaporator outlet [j/K.s]
Double precision Cc !Heat capacity rate of condenser [j/K.s]
Double precision Cco !Heat capacity rate of condenser outlet [j/K.s]
Double precision Cmin !Smaller or Ce and Cc [j/K.s]
Double precision Cmino !Smaller or Ce and Cc outlet [j/K.s]
Double precision Et !Overall effectiveness
Double precision Eto !Overall effectiveness outlet
Double precision een !Effectiveness of evaporator row
Double precision eeno !Effectiveness of evaporator row outlet
Double precision ecn !Effectiveness of condenser row
Double precision ecno !Effectiveness of condenser row outlet
Double precision ee !Effectiveness of evaporator
Double precision eeo !Effectiveness of evaporator outlet
Double precision ec !Effectiveness of condenser
Double precision eco !Effectiveness of condenser outlet
Double precision NTUe !Number of effectiveness units evaporator
Double precision NTUeo !Number of effectiveness units evaporator outlet
Double precision NTUc !Number of effectiveness units condenser
Double precision NTUco !Number of effectiveness units condenser outlet
Double precision Pr !Prandtl number evaporator
Double precision Preo !Prandtl number evaporator outlet
Double precision Prc !Prandtl number condenser
Double precision Prco !Prandtl number condenser outlet
Double precision Vmaxe !Maximum velocity evaporator [m/s]
Double precision Vmaxeo !Maximum velocity evaporator outlet [m/s]
Double precision Vmaxc !Maximum velocity condenser [m/s]
Double precision Vmaxco !Maximum velocity condenser outlet [m/s]
Double precision ReDe !Reynolds number evaporator
Double precision ReDeo !Reynolds number evaporator outlet
Double precision ReDc !Reynolds number condenser
Double precision ReDco !Reynolds number condenser outlet
Double precision Nuse !Nusselt number evaporator
Double precision Nuseo !Nusselt number evaporator outlet
Double precision Nusc !Nusselt number condenser
Double precision Nusco !Nusselt number condenser outlet
Double precision ve !Free flow velocity evaporator [m/s]
Double precision veo !Free flow velocity evaporator outlet [m/s]
Double precision vc !Free flow velocity condenser [m/s]
Double precision vco !Free flow velocity condenser outlet [m/s]
Double precision RHOe !Density evaporator fluid [kg/m3]
Double precision RHOeo !Density evaporator fluid outlet [kg/m3]
Double precision RHOc !Density condenser fluid [kg/m3]
Double precision RHOco !Density condenser fluid outlet [kg/m3]
Double precision Nue !Kinematic viscosity evaporator [m2/s]
Double precision Nueo !Kinematic viscosity evaporator outlet [m2/s]
Double precision NUC !Kinematic viscosity condenser [m2/s]
Double precision NUco !Kinematic viscosity condenser outlet [m2/s]
Double precision LAMDAe !Thermal conductivity evaporator fluid [W/m.K]
Double precision LAMDAeo !Thermal conductivity evaporator fluid outlet [W/m.K]
Double precision LAMDAC !Thermal conductivity condenser fluid [W/m.K]
Double precision LAMDACO !Thermal conductivity condenser fluid outlet [W/m.K]
Double precision SHCe !Specific heat capacity evaporator fluid [J/kg.K]
Double precision SHCeo !Specific heat capacity evaporator fluid outlet [J/kg.K]
Double precision SHCc !Specific heat capacity condenser fluid [J/kg.K]
Double precision SHCco !Specific heat capacity condenser fluid outlet [J/kg.K]
Double precision Timestep,Time !Simulation timestep and time [s]
Double precision PI !Pi, 3.1415927
Integer CurrentUnit, CurrentType

```

```

!Evaluation Of Pr At Wall Temperature
Double precision Pres !Pr evaluated at evaporator wall temperature
Double precision Prcs !Pr evaluated at condenser wall temperature
Double precision NUew !Kinematic viscosity at evaporator wall [m2/s]
Double precision NUCw !Kinematic viscosity at condenser wall [m2/s]
Double precision LAMDAew !Thermal conductivity at evaporator wall [W/m.K]
Double precision LAMDAcw !Thermal conductivity at condenser wall [W/m.K]
Double precision Twe !Iterating evap wall temperature to determine Pres [deg C]
Double precision Twc !Iterating cond wall temperature to determine Prcs [deg C]
Double precision SHCew !Specific heat capacity at evaporator wall temperature [J/kg.K]
Double precision SHCcw !Specific heat capacity at condenser wall temperature [J/kg.K]

!Goalseeking
Double precision Twe_up !Goalseek up function for Twe [deg C]
Double precision Twe_down !Goalseek down function for Twe [deg C]
Double precision Twc_up !Goalseek up function for Twc [deg C]
Double precision Twc_down !Goalseek down function for Twc [deg C]
Double precision Q1e !m.cp.dT
Double precision Q2e !((Thi-Tho)/log(Thi-Twe)/Tho-Twe)
Double precision Q4e !((Thi-Tho)/log(Thi-Twe(up/down))/Tho-Twe(up/down))
Integer numiterations
Double precision dQ1e !Q1e - Q2e
Double precision dQ2e !Q1e - Q4e
Double precision Q1c !m.cp.dT
Double precision Q2c !((Tco-Tci)/log(Tci-Tw)/Tco-Tw)
Double precision Q4c !((Tco-Tci)/log(Tci-Tw(up/down))/Tco-Tw(up/down))
Double precision dQ1c !Q1c - Q2c
Double precision dQ2c !Q1c - Q4c
Double precision Thog !Source outlet temperature initial guess [deg C]
Double precision Tcog !Sink outlet temperature initial guess [deg C]

!Finning influence
Double precision CF !Correction factor for Nusselt equations
Double precision efffe !Efficiency of the fin evaporator
Double precision efffc !Efficiency of the fin condenser
Double precision Afe !Heat transfer area of the evaporator fins [m2]
Double precision Afc !Heat transfer area of the condenser fins [m2]
Double precision xe !sqrt(2hfc/kfe*efffe)
Double precision xc !sqrt(2hfc/kfe*efffc)
Double precision kfe !Thermal conductivity of evaporator fin [W/m.K]
Double precision kfc !Thermal conductivity of condenser fin [W/m.K]
Double precision Lhle !Length of helical evaporator [m]
Double precision Lhlc !Length of helical condenser [m]

!Outputs
Double precision Tho !Temperature of source outlet fluid [deg C]
Double precision Tco !Temperature of sink outlet fluid [deg C]

```

Figure 15: Code to declare all the variables that Type202 uses throughout the subroutine.

After declaring the variables, the entirety of the code underneath is the executable section. Each line is read and executed sequentially. The variables *Time*, *Timestep*, *CurrentUnit*, *CurrentType* are global variables that are required to be read during each iteration to provide the transient nature output of the simulation.

The code needs to be ‘version signed’. This is done to inform the kernel which version of TRNSYS and therefore the convention in which the component was written. This alters how the kernel handles the component. This allows backward compatibility with components of TRNSYS written in earlier versions and will allow future compatibility with the next versions of TRNSYS. This step is vital as the simulation will call an error if the Type is not signed to a particular version.

On the last run through of the code, at the end of the simulation, it may be required to perform certain actions such as closing external files before returning control to the kernel. This is known as last call manipulation. No last call functions were required for Type202 so it was only necessary to return control to the kernel.

When a particular timestep finishes, every Type in the simulation is recalled. End of timestep manipulations allows functions to occur before the Type is recalled into the simulation. No end of timestep manipulations were required for Type202 so the *Return* function allows the Type to be recalled.

To operate correctly, the kernel needs to be told what Type202 is composed of. The code required informs the kernel that there are fifteen parameters, four inputs, zero derivatives and two outputs. The iteration mode tells the kernel how often the type should be called. A value of one indicates that Type202 should be called at every timestep regardless of whether the input values have altered to the previous iteration. The number of stored variables sets the required number of static and dynamic storage spots. Type202 completes a calculation every timestep with the inputs and so no stored variables are required. No discrete controls are required.

The code assigns units to the input and output values. This is an extremely important step to avoid inadvertently performing calculations or connecting components with different units. A good example of this is whether the component calculates using Kelvin or degrees Celsius. If an output value of one parameter is in a different unit to another, as long as the measurement type is the same (e.g. temperature), TRNSYS will convert the value to the correct unit. The programmer's manual provides a breakdown of the available measurement types, the units, the TRNSYS code and the mathematical conversion used.

On the first run of the code there are no iterations, but the initial input and output values of the parameters are read. The initial parameter values are read from external data files or component input values. The order within the component determines the number assigned to it. The *JFIX* function is used to ensure the number read is an integer.

If an out of range parameter is found, to prevent erroneous and incorrect calculations, error messages were built into the code. If a parameter is out of range and the simulation is run, an error message pops up. This is essential to ensure all the parameters are correctly input and

results are obtained incorrectly. Figure 16 shows the coded ranges with the error messages that are shown in a pop-up box and the results file if out of range parameters are input.

In this case:

- The number of rows (N_r) in the HPHE had to be greater than one. The input defaults to zero. This was to ensure that an input was in place.
- It is easy to input the outer diameter of the pipe in millimetres or centimetres rather than metres. If D_{out} was over one, it was obvious that the incorrect unit and therefore input was used.
- As the initial default value of the length of the evaporator (L_e) and length of the condenser (L_c) was zero, ensuring that L_e and L_c were greater than zero ensured that a value was input in the initial parameters.
- To ensure the number of heat pipes in a row (N_t) was input, an error occurred if the value was less than or equal to zero.
- To ensure the distance between the heat pipes rows and the heat pipe centres in a row (ST and SL) was input in metres, a value greater than or equal to one gave an error.
- To ensure an input was given for the flow area of the evaporator and condenser (A_e and A_c), a value less than or equal to zero gave an error.
- The finning mode depends on whether the evaporator or condenser sections were finned. 1= no finning, 2= condenser finned, 3= evaporator finned, 4= both finned. Inputs outside of 1-4 are not allowed.
- The fluid mode told the component which heat sink was being used. 1= air, 2= water 3= thermal oil. Inputs outside of 1-3 are not allowed.
- Errors for the finning parameters ensured measurements were in input in metres.

```

!Check Parameters for Problems
If (Nr <= 1) Call FoundBadParameter(1, 'Fatal', 'The number of rows must be positive.')
If (Dout > 1.d0) Call FoundBadParameter(2, 'Fatal', 'Ensure diameter is in metres')
If (Le <= 0.d0) Call FoundBadParameter(3, 'Fatal', 'The length evaporator must be positive.')
If (Lc <= 0.d0) Call FoundBadParameter(4, 'Fatal', 'The length condenser must be positive.')
If (Nt <= 0.d0) Call FoundBadParameter(5, 'Fatal', 'Number of heat pipes in row must be positive.')
If (ST >= 1.d0) Call FoundBadParameter(6, 'Fatal', 'Ensure distance between rows is in metres')
If (SL >= 1.d0) Call FoundBadParameter(7, 'Fatal', 'Ensure distance between heat pipes is in metres')
If (Ae <= 0.d0) Call FoundBadParameter(8, 'Fatal', 'Ae must be positive')
If (Ac <= 0.d0) Call FoundBadParameter(9, 'Fatal', 'Ac must be positive')
If ((FinningMode <= 0) .or. (FinningMode > 4)) Call FoundBadParameter(10, 'Fatal', 'Finning mode must be between 1 and 4')
If ((FluidMode <= 0) .or. (FluidMode > 3)) Call FoundBadParameter(11, 'Fatal', 'Fluid mode must be between 1 and 3')
If (Dofin >= 1) Call FoundBadParameter(12, 'Fatal', 'Ensure fin diameter is in metres')
If (efin >= 1) Call FoundBadParameter(13, 'Fatal', 'Ensure outer fin diameter is in metres')
If (Pfin >= 1) Call FoundBadParameter(14, 'Fatal', 'Ensure pitch is in metres')
If (Hfin >= 1) Call FoundBadParameter(15, 'Fatal', 'Ensure fin height is in metres')
If (ErrorFound()) Return

```

Figure 16: Code to provide error notification if parameters are outside correct ranges for calculations to function.

At the first timestep the outputs of the simulation need an initial value. In this case the output values were set to the values of Tho and Tco; temperature of the hot and cold stream outlets.

In a simulation, it is possible to run multiples of the same Type. For example, if multiple HPHEs are in a simulation, multiple Type202 components will be put into the simulation. The simulation needs to treat these Types separately. For this reason, there is a dedicated code for multiple unit manipulation. *If (getIsReReadParameters())* is the function used that causes the parameters list to be reread if there is more than one Type in a simulation.

There are four inputs for Type202, namely: temperatures and mass flow rates of the source and sink inlet streams. As with the parameters, the inputs need to be in range for a successful calculation and to check that they have been entered. For this reason, error messages were coded (Figure 17) to ensure the simulation was not run if this was the case.

```

If (Thi < 0.) Call foundBadInput(1, 'Fatal', 'The source inlet temperature must be positive')
If (Tci < 0.) Call foundBadInput(2, 'Fatal', 'The sink inlet temperature must be positive')
If (FLWe < 0.) Call foundBadInput(3, 'Fatal', 'The source inlet flow rate must be positive')
If (FLWc < 0.) Call foundBadInput(4, 'Fatal', 'The sink inlet flow rate must be positive')
If (ErrorFound()) Return

```

Figure 17: Code to provide an error notification if out of range inputs are entered.

All the internal calculations then occur. After all the internal calculations, the final values for Tho and Tco are calculated. At each iteration, Tho and Tco are set as visualisable output values. These values are stored in the memory and can be used at the next timestep. *End Subroutine* is then used to return control to the kernel after all the calculations are completed and the values are stored. The subroutine for Type202 is then ended.

4.1.2 Creating a *.dll File Using Intel Visual Fortran 19

The TRNSYS Programmer's Guide [62] is slightly outdated as the manual only provides instructions on how to add a Type to the TRNDLL.dll using Intel Visual Fortran 11. This process was done using Intel Visual Fortran 19 and so it varied from the instructions given in the manual. The instructions to add a new project to the Ivfl1.x solution is provided in this section by a flowchart for the process, Figure 18.

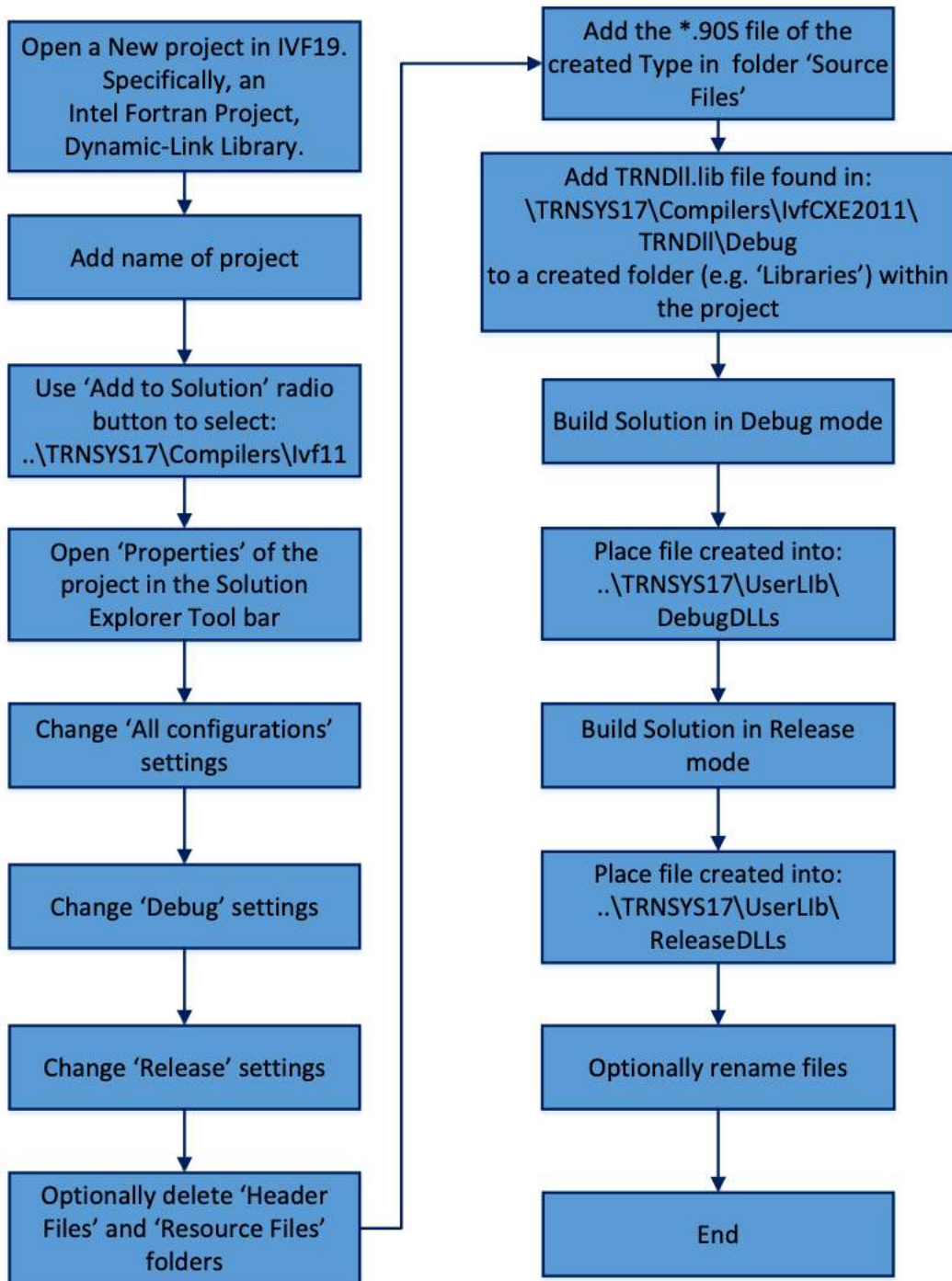


Figure 18: Flowchart for the process of compiling a component into a *.dll file to be used in TRNSYS.

4.1.3 HPHE Type202 Component Skeleton

A Type that is used for a simulation consists of two parts, the internal code that tells the component how to work, as detailed in Section 4.1.1 HPHE Coding, as well as the ‘skeleton’, which is used to enter the component into the simulation, link the component with other components in the simulation, house the code and provide parameter and input values. The

empty skeleton for Type 202 (HPHE) was created in Simulation Studio by pressing File>New>New Component (TRNSYS TYPE). A view of the final skeleton with all inputted data for the General, Parameter, Input and Output tab pages are provided in Figure 19 to Figure 22, respectively.

The screenshot shows the 'General' tab of a component configuration window. The tabs at the top are 'General', 'Description', 'Variables', and 'Files'. The 'General' tab is active and contains the following fields and options:

- Object:** Counterflow Heat Pipe Heat Exchanger
- Author:** Daniel Brough
- Organization:** Brunel University London
- Editor:** (empty field)
- Creation Date:** January 02, 2020
- Last Modification:** March 13, 2020
- Model Type:** Radio buttons for Detailed, Simplified, Empirical (selected), and Conventional.
- Validation:** Checkboxes for Qualitative, Analytical, Numerical, Experimental (checked), and In Assembly.
- Type Number:** 202
- Allowed Instances:** (empty field)
- KeyWords:** (empty text area)
- Buttons:** Add, Del, and Choose icon ...
- Icon:** -E.bmp (Command)

Figure 19: View of 'General' tab for HPHE component in Simulation Studio.

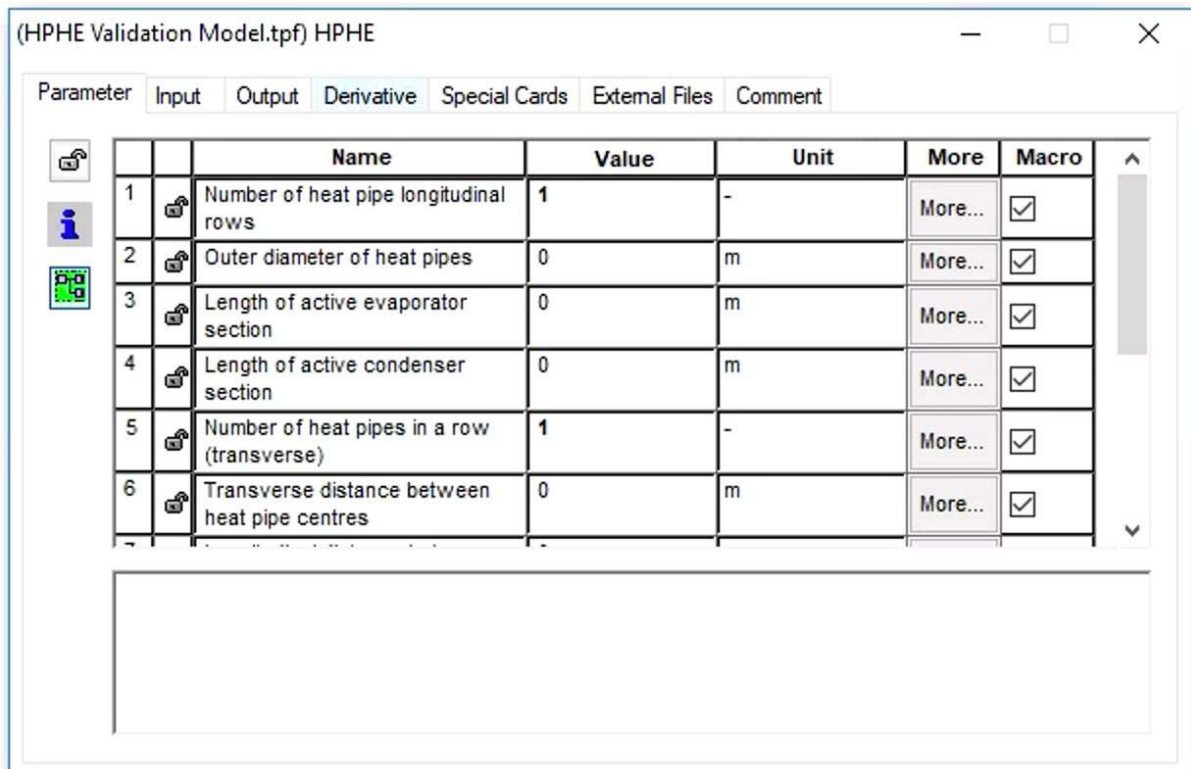


Figure 20: View of Type202 component 'Parameter' tab in Simulation Studio.

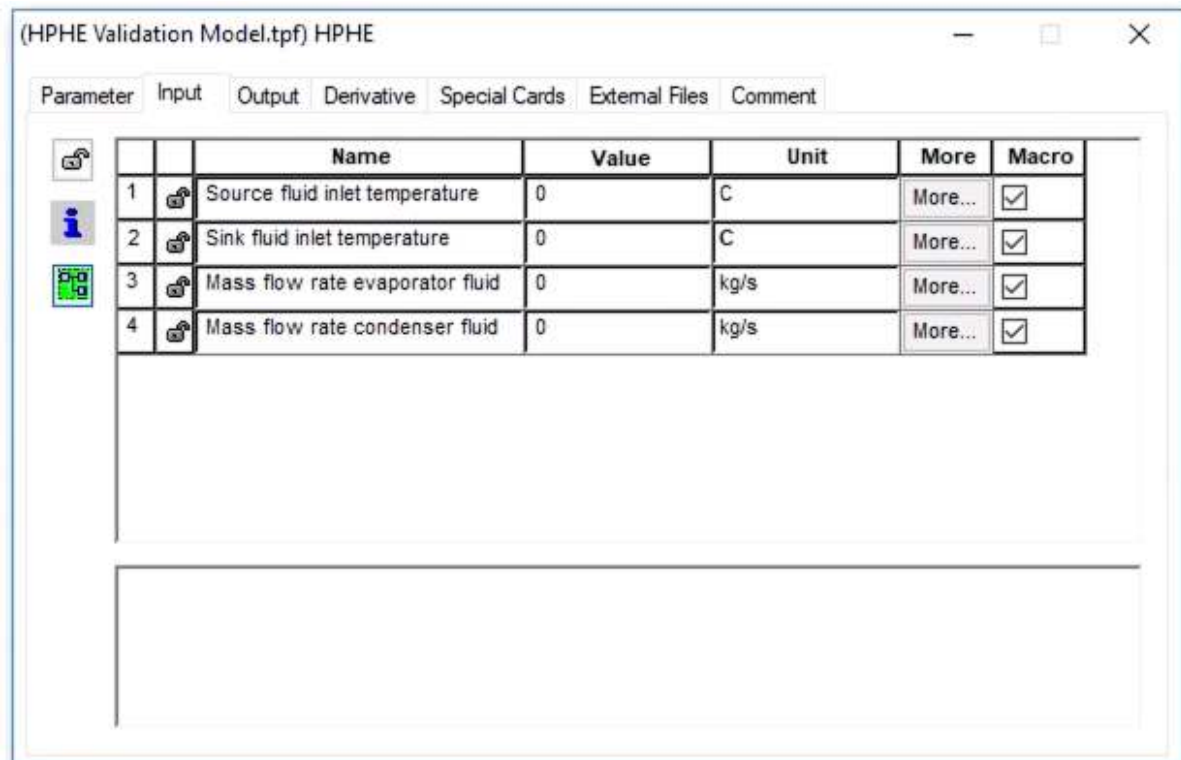


Figure 21: View of Type202 component 'Input' tab in Simulation Studio.

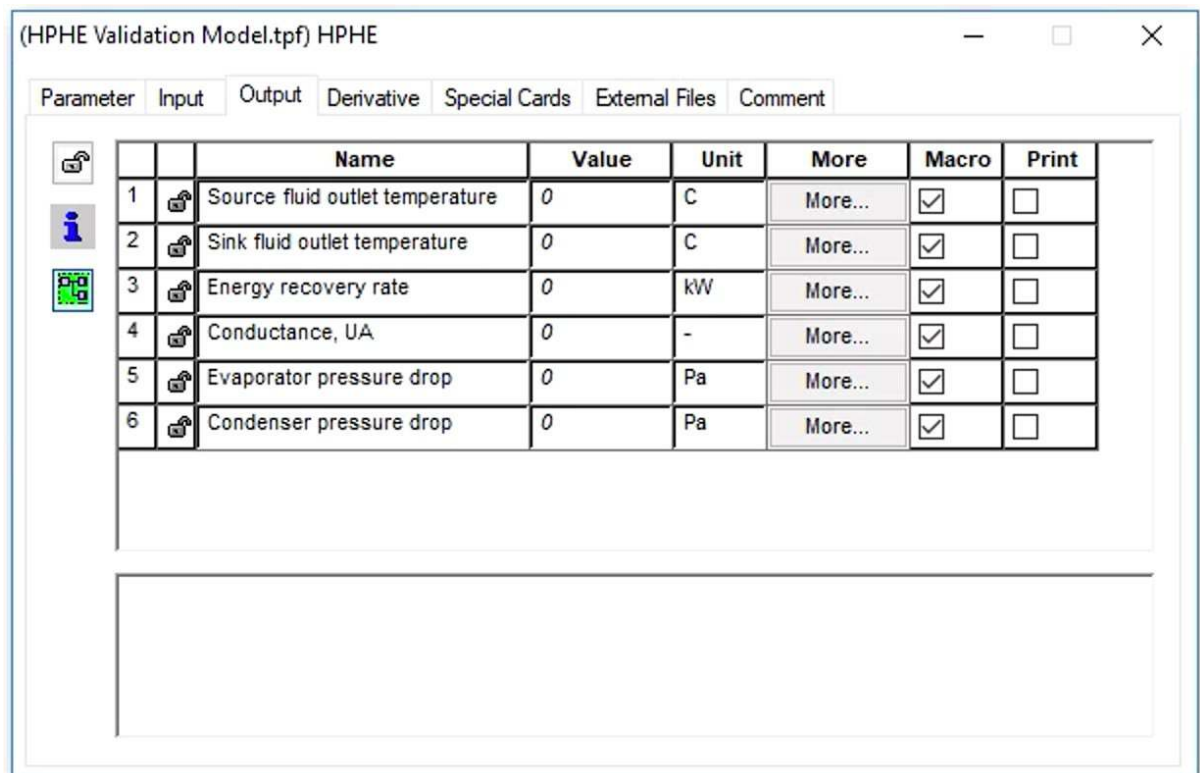
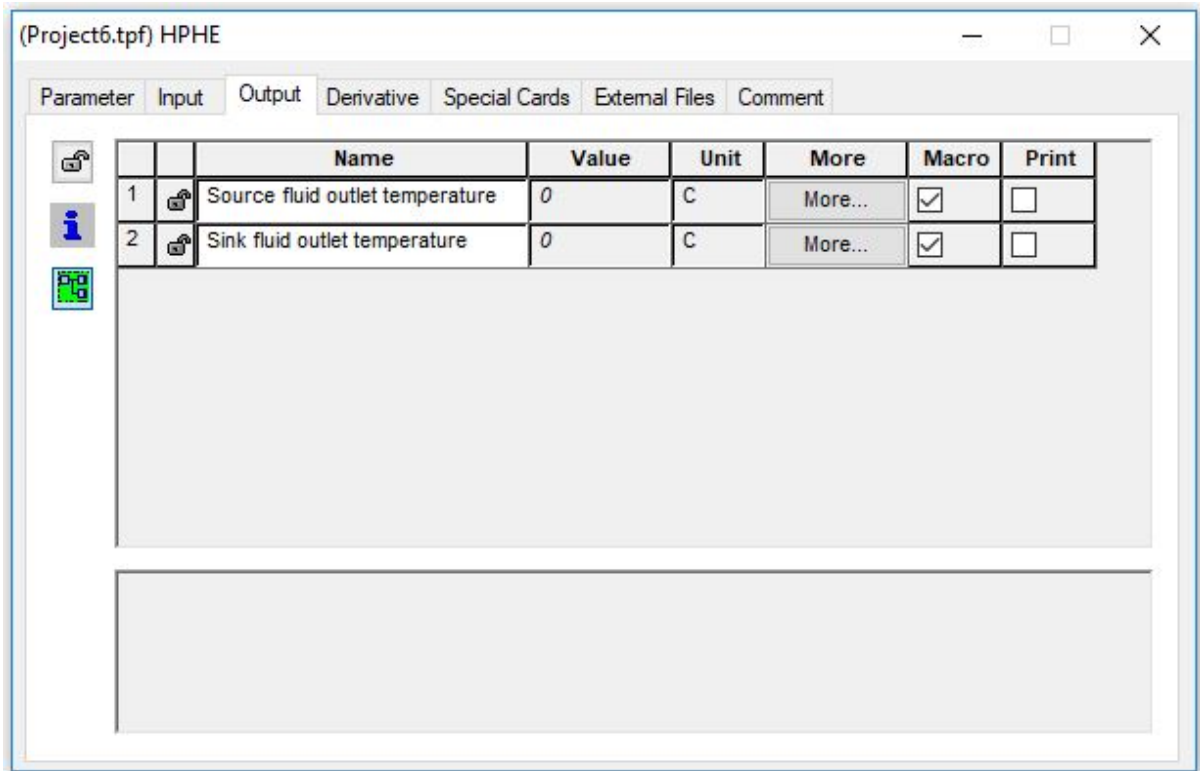


Figure 22: View of Type202 component 'Output' tab in Simulation Studio.

4.1.4 Model Limitations

There are several limitations to this model. Firstly, it does not take into account start-up of the heat pipes. It assumes start-up is achieved and the heat pipes are operational. In saying this, the model is used to determine recovered heat energy in a process system that would be operational, so start-up is not essential.

Secondly, HPHEs have thermal inertia. For example, there is residual heat in the casing of the HPHE and the heat pipes themselves that will be transferred to the sink fluid if the source stream is cooling down. Axial conduction through the heat pipe and conduction through the separation plate is also present. These factors are not taken into account. This means the model adapts more quickly than what would occur in reality, as witnessed in the results.

The model assumes perfect insulation whereas the HPHE loses heat through the casing. As such, the model slightly overpredicts the performance, as seen in the results. It is possible to predict temperature loss from the HPHE casing based on the design parameters. However, it was deemed unnecessary as many additional parameters would have to be input and would make the model much more cumbersome for little return.

The Type, currently, only provides outlet data about the temperature. Additional work is being undertaken to provide, for example, pressure drop, energy recovery rate and conductance values.

Currently, only helical finning is available as an option, whereas, in reality, other configurations are possible. Future work can be undertaken to validate other configurations, and the code can be updated accordingly.

4.2 Experimental Unit

The HPHE unit that was used to validate the model was installed to recover energy from the cooling section of a ceramic continuous roller kiln used to fire tiles. Further information on this exhaust-air HPHE can be found in Ref. [63]. Figure 23 and Figure 24 provide the 3D drawing of the HPHE unit and the dimensions. Figure 25 provides the detail of the separation plate between the two streams and the heat pipe arrangement.

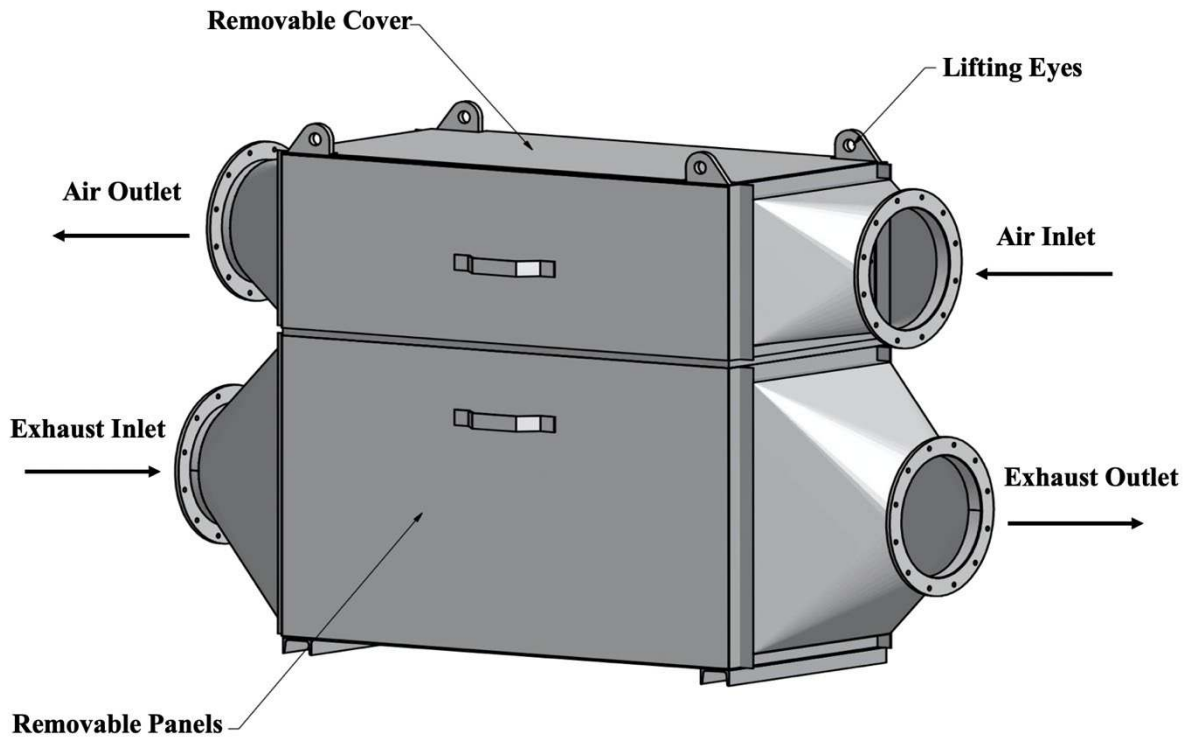


Figure 23: 3D schematic of the HPHE.

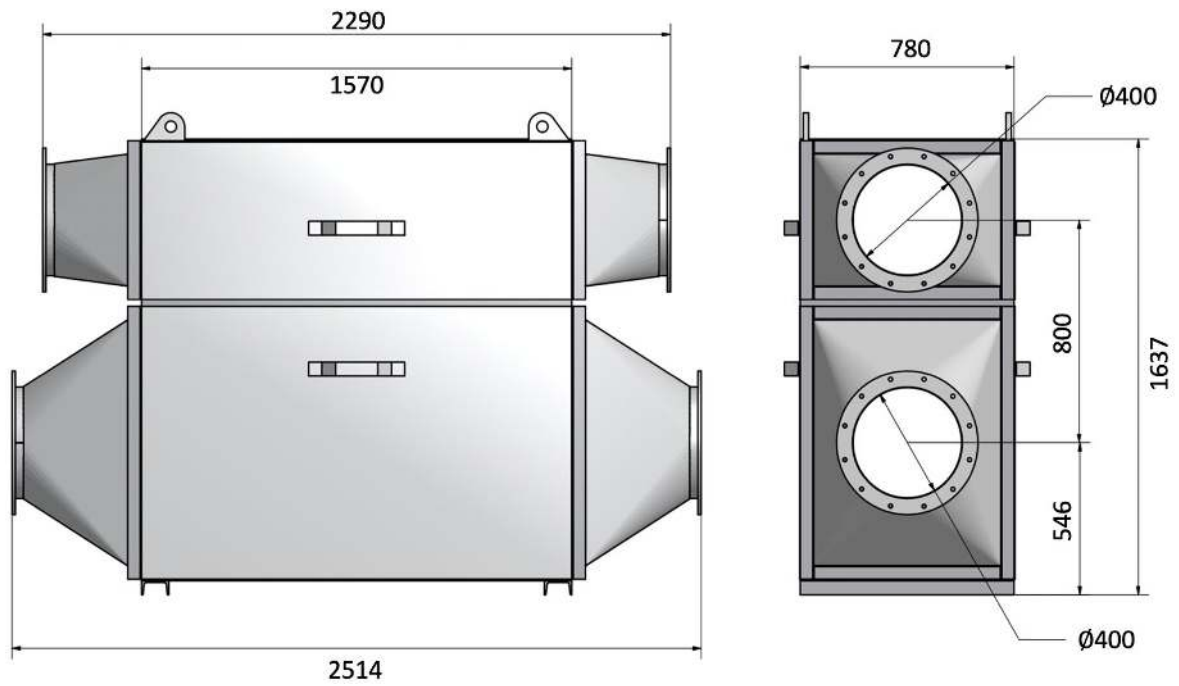


Figure 24: Dimensions of the HPHE.

NO OF ROWS: 18
 HOLES PER ROW 9
 TOTAL NO. OF HOLES: 162

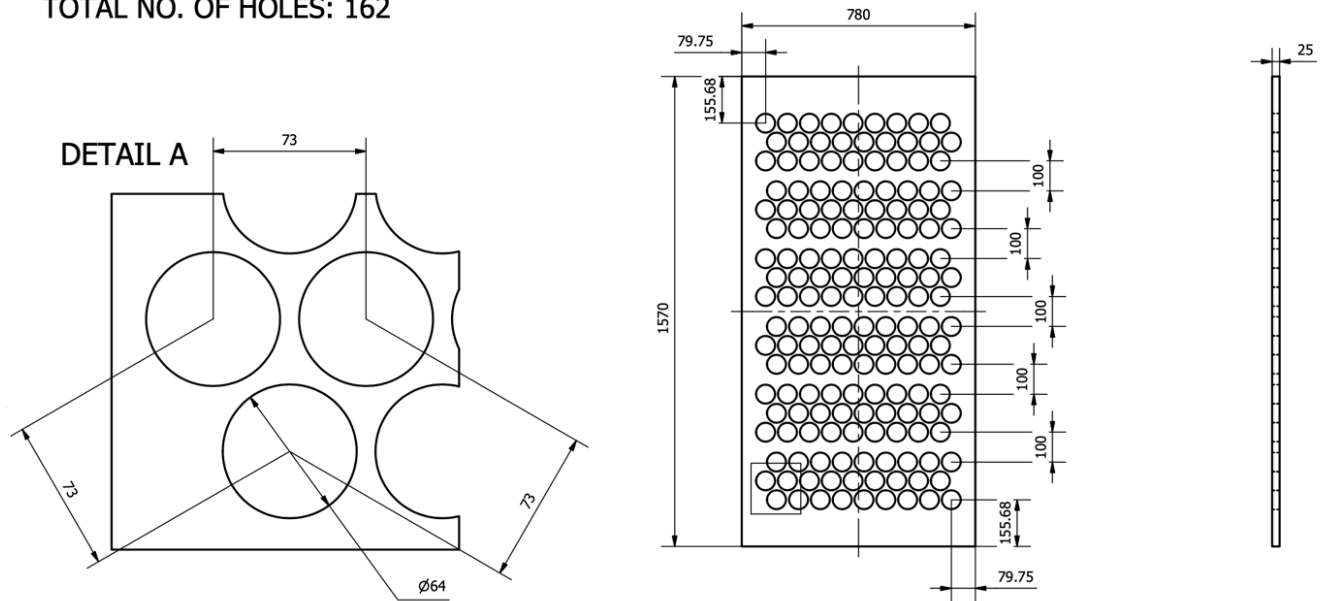


Figure 25: Separation plate and heat pipe arrangement detail.

Figure 26 shows the inlet flow rate data from the experimental HPHE. There was the inlet of the exhaust to the evaporator section and the inlet of the air to the condenser. A data point was taken every minute. 1300 minutes of data were used. Data for flow rate were measured in $\text{Nm}^3.\text{hr}^{-1}$, which had to be converted to $\text{kg}.\text{hr}^{-1}$ for the TRNSYS simulation. This was achieved using the ideal gas law equation as done by [45]. There were fluctuations in the data mainly in the exhaust flow rate. A maximum error of mass flow rate of 2.78% was reported. The average values for the exhaust and air inlet flow rate were 6047 and 2600 $\text{kg}.\text{hr}^{-1}$, respectively. The maximum and minimum flow rates for the exhaust were 6869 and 632 $\text{kg}.\text{hr}^{-1}$ and for the air were 2644 and 2560 $\text{kg}.\text{hr}^{-1}$. These fluctuations assisted in showing that the model would adapt to fluctuating conditions.

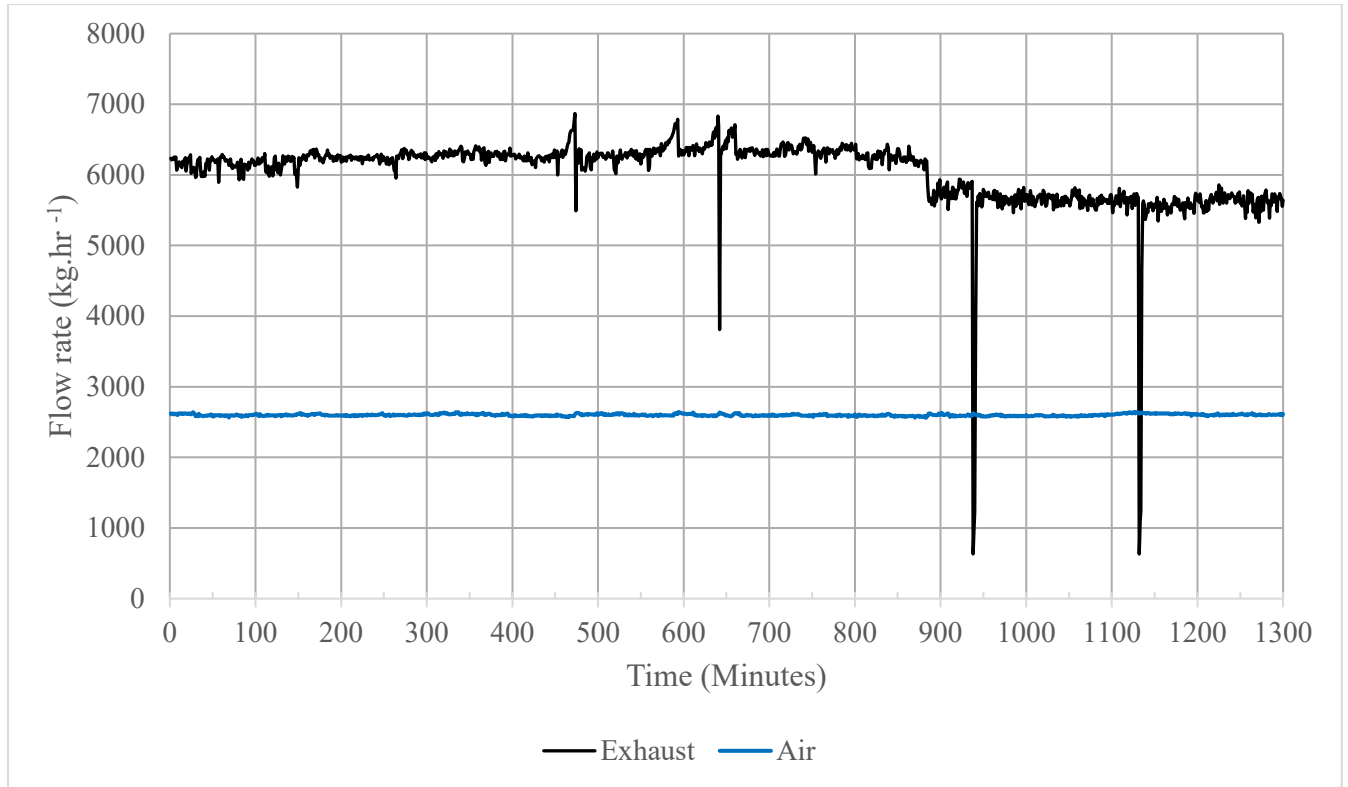


Figure 26: Graph showing the inlet flow rate of the exhaust and air streams.

4.3 Model for Validation

Figure 27 shows the model built to validate the component. The left highlighted box shows the real-world experimental data input into the model. These are connected to the HPHE Type that does the mathematical operation. The outputs of the Type are sent to a plotter to graphically display the results. Table 5 gives further information on each Type used in the simulation.

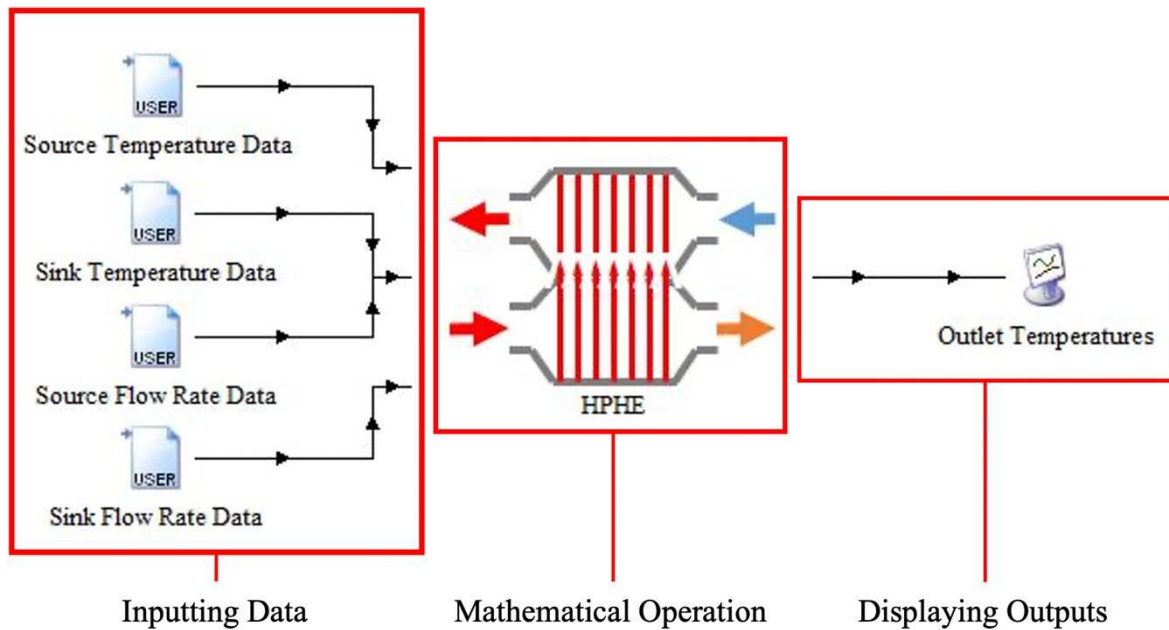

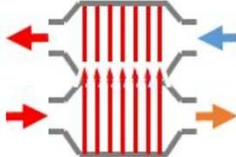



Figure 27: Labelled model in Simulation Studio.

Table 5: Components used in the TRNSYS model, their Type and description.

| Component | Type | Description |
|---|----------|------------------------------------|
|  | Type 9a | Data reader for generic data files |
|  | Type 202 | HPHE component developed. |
|  | Type 65 | Online Graphical Plotter |

5 Results and Discussion

5.1 Comparison of Results

Figure 28 shows the experimental inlet and outlet temperature data of the installed HPHE. The inlet temperatures were fed into the model and the outlet temperatures were used for comparison against the

simulation to validate the component. Figure 29 shows the graph produced in TRNSYS of the simulation inlet and outlet temperatures of the source and sink fluids for comparison.

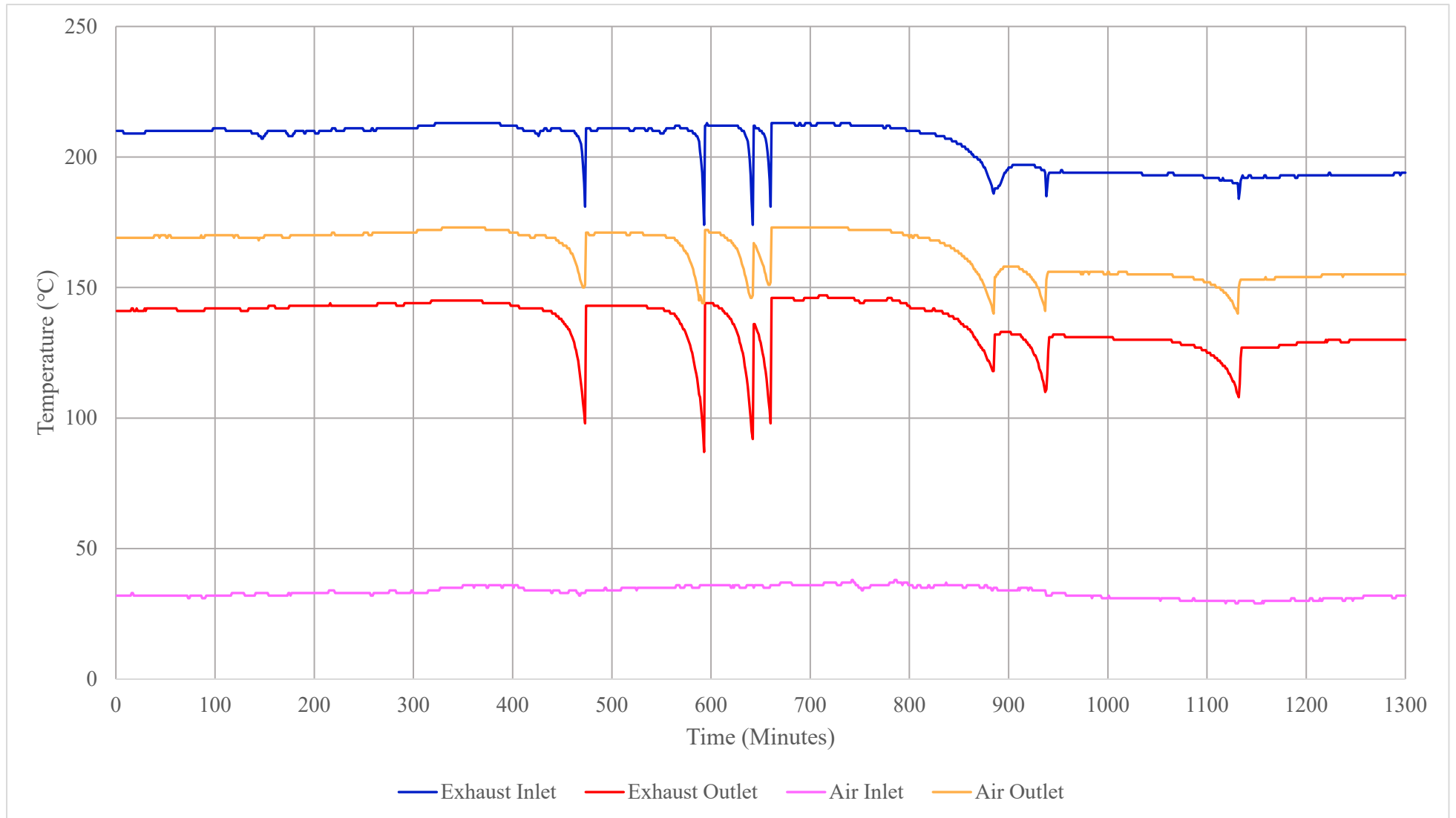


Figure 28: A graph showing the experimental inlet and outlet temperatures of the source and sink fluids.

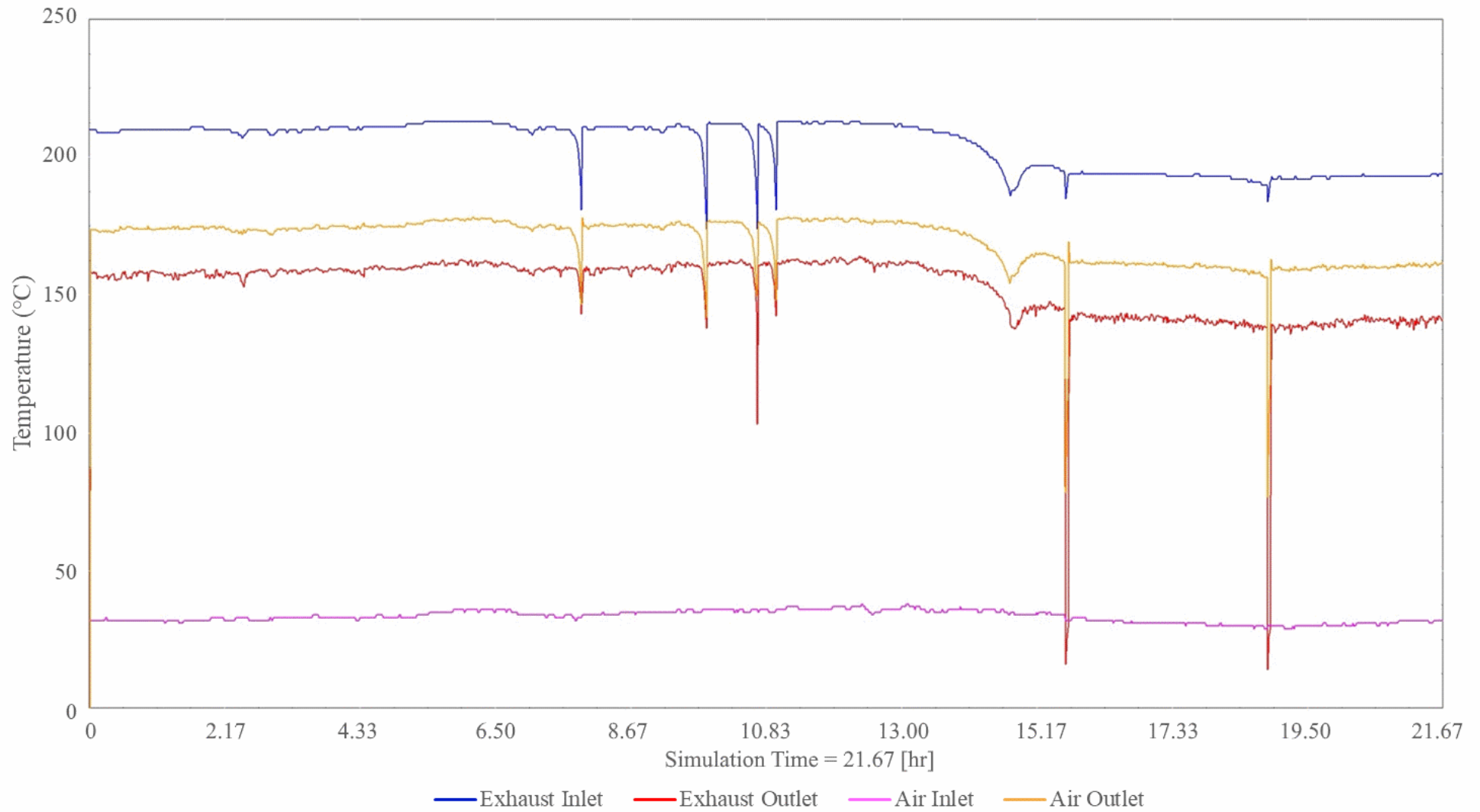


Figure 29: A graph showing the simulation inlet and outlet temperatures of the source and sink fluids.

In the experiments, the air inlet is roughly 35°C and rises to between 150-175°C depending on the flow rate. The exhaust drops from between 190-210°C to 130-145°C.

In the simulation, the air and exhaust inlets directly relate to the experimental set up as these were used as the inputs. The air outlet rose to between 160-175°C and the exhaust dropped to between 140-160°C. It can be seen by comparing the graphs that the simulation follows the experimental results very similarly.

5.2 Energy Recovery Comparison

The energy recovered was calculated from the secondary stream, air, using:

$$\dot{Q} = \dot{m} c_p \Delta T \quad (5.1)$$

The energy recovery of the experiment was plotted against the simulation for comparison, shown in Figure 30. It is seen that most results fall well within a $\pm 15\%$ difference with a few outliers predominantly caused by the faster response of the simulation compared to the experiment and lack of thermal inertia. The simulation slightly overpredicted the performance of the HPHE, this is as expected as the model assumes perfect insulation, with no energy losses. Also, with the large number of variables and extensive calculations that need to be conducted, this performance is more than acceptable. The errors between simulation and experiment were rounded and a histogram plot (Figure 31) shows the spread of error with the majority falling between 3-4%. Six major outliers, circled in red, in Figure 30 were removed and the average error was 4.4%.

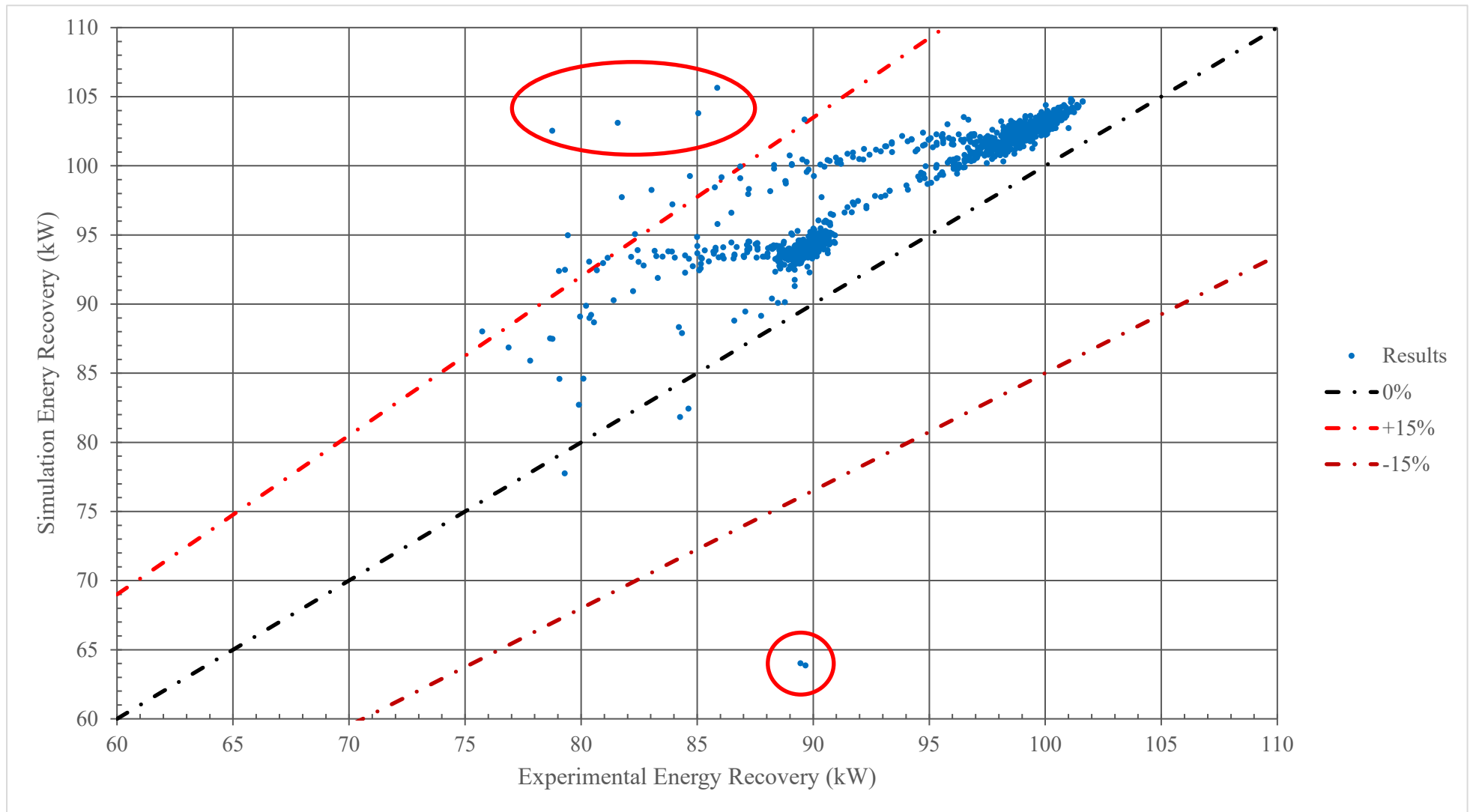


Figure 30: A comparison of energy recovery between experimental and simulation results.

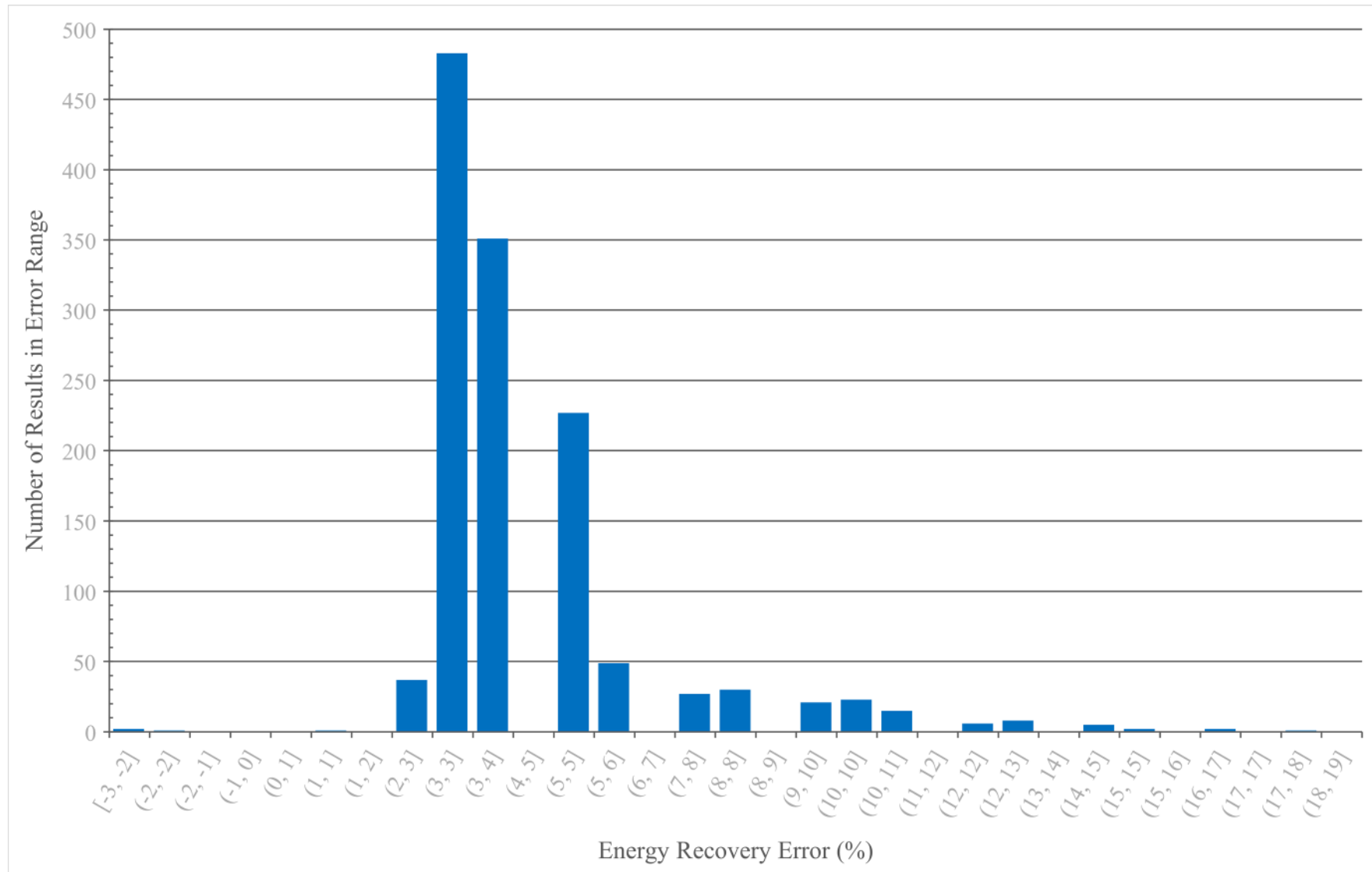


Figure 31: A histogram plot of percentage error.

6 Conclusion

A TRNSYS Type has been built to simulate a counter-flow HPHE component that provides accurate predictions on outlet temperatures of both the source and sink fluid. This was done using the ϵ -NTU method and real-world installation data. The results of the simulation were well within $\pm 15\%$, with an average of 4.4% error, compared to the experimental results. This component can now be used confidently in larger waste heat recovery system simulations that encompass a HPHE of this configuration. Furthermore, transient HPHE calculations are now possible whereas previously averaged fixed values would have to be used as inputs. Future work will be required to ensure the method of calculating ϵ_t is applicable to further applications. Now the component has been validated, the TRNSYS performance of an entire system including a HPHE can be simulated to determine the system performance over time and aid the design and installation of HPHEs for the purpose of WHR. In this paper, an exhaust gas to air unit was validated using an available full-scale unit. Further full-scale units that are currently being installed will be used to validate thermal oil and water as heat sinks, once sufficient data has been collected, in a future article. Methods will be included for determining pressure drop as well as conductance values and energy recovery rate as outputs of the model.

7 Acknowledgements

The research presented in this paper has received funding from the European Union's H2020 programme ETEKINA and DREAM under grant agreement numbers 768772 and 723641, respectively. The authors acknowledge further support of research funding contributed by JBM International.

8 References

- [1] H. Ritchie and M. Roser, "CO₂ and Greenhouse Gas Emissions," Our World in Data, December 2019. [Online]. Available: <https://ourworldindata.org/co2-and-other-greenhouse-gas-emissions>. [Accessed 26 April 2020].
- [2] United Nations Secretary-General, "Report of the Secretary-General on the 2019 Climate Action Summit," United Nations, 2019.

- [3] United Nations Treaty Collection, “Paris Agreement Chapter XXVII environment,” United Nations, New York, 2015.
- [4] European Commission, “2030 climate & energy framework,” [Online]. Available: https://ec.europa.eu/clima/policies/strategies/2030_en. [Accessed 24 April 2020].
- [5] J. Malinauskaite, H. Jouhara, L. Ahmad, M. Milani, L. Montorsi and M. Venturelli, “Energy efficiency in industry: EU and national policies in Italy and the UK,” *Energy*, vol. 172, pp. 255-269, April 2019. <https://doi.org/10.1016/j.energy.2019.01.130>.
- [6] Central Intelligence Agency, “The World Factbook 2016/17,” New Zealand, 2016.
- [7] A. Simeone, Y. Luo, E. Woolley, S. Rahimifard and C. Boër, “A decision support system for waste heat recovery in manufacturing,” *CIRP Annals*, vol. 65, no. 1, pp. 21-24, 2016. <https://doi.org/10.1016/j.cirp.2016.04.034>.
- [8] H. Jouhara and A. G. Olabi, “Editorial: Industrial waste heat recovery,” *Energy*, vol. 160, pp. 1-2, 2018. <https://doi.org/10.1016/j.energy.2018.07.013>.
- [9] D. Brough and H. Jouhara, “The aluminium industry: A review on state-of-the-art technologies, environmental impacts and possibilities for waste heat recovery,” *International Journal of Thermofluids*, Vols. 1-2, p. 100007, 2020. <https://doi.org/10.1016/J.IJFT.2019.100007>.
- [10] D. Reay and P. Kew, *Heat pipes: Theory, Design and Applications*, Elsevier Limited, 2006.
- [11] A. Faghri, “Heat pipes: Review, Opportunities and Challenges,” *Frontiers in Heat Pipes*, vol. 5, no. 1, pp. 1-48, 2014. <https://doi.org/10.5098/fhp.5.1>.
- [12] L. Vasiliev, “Heat pipes in modern heat exchangers,” *Applied Thermal Engineering*, no. 25, pp. 1-19, 2005. <https://doi.org/10.1016/J.APPLTHERMALENG.2003.12.004>.
- [13] Y. Çengel, *Heat Transfer: A Practical Approach* 2nd edition, McGraw-Hill, 2002.
- [14] W. M. Kays and A. L. London, *Compact Heat Exchangers* 3rd ed., New York: McGraw-Hill, 1984.

- [15] H. Jouhara, "4.3 Heat Pipes," *Comprehensive Energy Systems*, vol. 4, pp. 70-97, 2018. <https://doi.org/10.1016/b978-0-12-809597-3.00403-x>.
- [16] H. Jouhara, A. Chauhan, T. Nannou, S. Almahmoud, B. Delpech and L. Wrobel, "Heat pipe based systems - Advances and applications," *Energy*, vol. 128, pp. 729-754, 2017. <http://dx.doi.org/10.1016/j.energy.2017.04.028>.
- [17] A. Mehmood, A. Waqas, Z. Said, S. M. A. Rahman and M. Akram, "Performance evaluation of solar water heating system with heat pipe evacuated tubes provided with natural gas backup," *Energy Reports*, vol. 5, no. 1, pp. 1432-1444, 2019. <https://doi.org/10.1016/j.egy.2019.10.002>.
- [18] H. Hussein, "Theoretical and experimental investigation of wickless heat pipes flat plate solar collector with cross flow heat exchanger," *Energy Conversion and Management*, vol. 48, no. 4, pp. 1266-1272, 2007. <https://doi.org/10.1016/j.enconman.2006.09.021>.
- [19] H. Jouhara, J. Milko, J. Danielewicz, M. Sayegh, M. Szulgowska-Zgrzywa, J. Ramos and S. Lester, "The performance of a novel flat heat pipe based thermal and PV/T (photovoltaic and thermal systems) solar collector that can be used as an energy-active building envelope material," *Energy*, vol. 108, no. 1, pp. 148-154, 2016. <http://dx.doi.org/10.1016/j.energy.2015.07.063>.
- [20] G. Morrison and I. Budihardjo, "Performance of water-in-glass evacuated tube solar water heaters," *Solar Energy*, vol. 83, no. 1, pp. 49-56, 2009. <http://dx.doi.org/10.1016/j.solener.2008.06.010>.
- [21] H. Jouhara, V. Anastasov and I. Khamis, "Potential of heat pipe technology in nuclear seawater desalination," *Desalination*, vol. 249, no. 3, pp. 1055-1061, 2009. <http://dx.doi.org/10.1016/j.desal.2009.05.019>.
- [22] X. Zhang, Y. Liu, X. Wen, C. Li and X. Hu, "Low-grade waste heat driven desalination with an open loop heat pipe," *Energy*, vol. 163, pp. 221-228, 2018. <https://doi.org/10.1016/j.energy.2018.08.121>.
- [23] K. Kerrigan, H. Jouhara, G. O'Donnell and A. Robinson, "Heat pipe-based radiator for low grade geothermal energy conversion in domestic space heating," *Simulation*

Modelling Practice and Theory, vol. 19, no. 4, pp. 1154-1163, 2011.
<http://dx.doi.org/10.1016/j.simpat.2010.05.020>.

- [24] L. Ayompe, A. Duffy, M. Mc Keever, M. Conlon and S. McCormack, “Comparative field performance study of flat plate and heat pipe evacuated tube collectors (ETCs) for domestic water heating systems in a temperate climate,” *Energy*, vol. 36, no. 5, pp. 3370-3378, 2011. <http://dx.doi.org/10.1016/j.energy.2011.03.034>.
- [25] Etekina - Thermal Energy Recovery, 22 April 2020. [Online]. Available: <https://www.etekina.eu/>. [Accessed 26 April 2020].
- [26] B. Egilegor, H. Jouhara, J. Zuazua, F. Al-Mansour, K. Plesnik, L. Montorsi and L. Manzini, “ETEKINA: Analysis of the potential for waste heat recovery in three sectors: aluminium low pressure die casting, steel sector, and ceramic tiles manufacturing sector,” *International Journal of Thermofluids*, Vols. 1-2, February 2020. <https://doi.org/10.1016/j.ijft.2019.100002>.
- [27] B. Delpech, B. Axcell and H. Jouhara, “Experimental investigation of a radiative heat pipe for waste heat recovery in a ceramics kiln,” *Energy*, vol. 170, pp. 636-651, 2019. <https://doi.org/10.1016/j.energy.2018.12.133>.
- [28] I-ThERM, 21 May 2019. [Online]. Available: <http://www.itherm-project.eu/>. [Accessed 26 April 2020].
- [29] P. Dunn and D. A. Reay, *Heat Pipes* 3rd edition, Pergamon Press, 1982.
- [30] J. Kim and S. J. Kim, “Experimental investigation on working fluid selection in a micro pulsating heat pipe,” *Energy Conversion and Management*, vol. 205, p. 112462, 2020. <https://doi.org/10.1016/j.enconman.2019.112462>.
- [31] Heat Transfer Committee, “Convective Heat Transfer During Forced Crossflow of Fluids Over a Circular Cylinder, Including Free Convection Effects,” ESDU 69004a, 1970.
- [32] S. Almahmoud, *Experimental and theoretical investigation of a radiative flat heat pipe based heat exchanger for waste recovery in the steel industry*, Mechanical, Aerospace and Civil Engineering: Brunel University London, 2019.

- [33] E. Azad, "Theoretical and experimental investigation of heat pipe solar collector," *Experimental Thermal and Fluid Science*, vol. 32, no. 8, pp. 1666-1672, 2008. <https://doi.org/10.1016/j.expthermflusci.2008.05.011>.
- [34] H. Mroue, J. Ramos, L. Wrobel and H. Jouhara, "Experimental and numerical investigation of an air-to-water heat pipe-based heat exchanger," *Applied Thermal Engineering*, vol. 78, pp. 339-350, 2015. <http://dx.doi.org/10.1016/j.applthermaleng.2015.01.005>.
- [35] J. Ramos, A. Chong and H. Jouhara, "Experimental and numerical investigation of a cross flow air-to-water heat pipe-based heat exchanger used in waste heat recovery," *International Journal of Heat and Mass Transfer*, vol. 102, pp. 1267-1281, 2016. <https://doi.org/10.1016/j.ijheatmasstransfer.2016.06.100>.
- [36] W. S. Chang and G. T. Colwell, "Mathematical Modeling of the Transient Operating Characteristics of Low-Temperature Heat Pipe," *Numerical Heat Transfer*, vol. 8, pp. 169-186, 1985. <https://doi.org/10.1080/01495728508961848>.
- [37] J. E. Deverall, J. E. Kemme and L. W. Florschuetz, "Sonic Limitations and Startup Problems of Heat Pipes," NASA, Los Alamos, 1970.
- [38] G. T. Colwell, "Modeling of Transient Heat Pipe Operation," Langley Research Centre, NASA, Hampton, Virginia 23665, 1989. <https://ntrs.nasa.gov/archive/nasa/casi.ntrs.nasa.gov/19890010131.pdf>.
- [39] L. Yang, X. Ling, H. Peng, L. Duan and X. Chen, "Starting characteristics of a novel high temperature flat heat pipe receiver in solar power tower plant based of "Flat-front" Startup model," *Energy*, vol. 183, pp. 936-945, 2019. <https://doi.org/10.1016/j.energy.2019.07.007>.
- [40] J.-M. Tournier and M. S. El-Genk, "A heat pipe transient analysis model," *International Journal of Heat and Mass Transfer*, vol. 37, no. 5, pp. 753-762, 1994. [https://doi.org/10.1016/0017-9310\(94\)90113-9](https://doi.org/10.1016/0017-9310(94)90113-9).
- [41] P. Brocheny, *Modeling of the Transient Behavior of Heat Pipes with Room-Temperature Working Fluids*, 10: Tigerprints, 2006.

- [42] I. Budihardjo, G. Morrison and M. Behnia, "Development of TRNSYS Models for Predicting the Performance of Water-in-Glass Evacuated Tube Solar Water Heaters in Australia," in *Destination Renewables - ANZSES*, 2003.
- [43] Y. Yau and A. Tucker, "The performance study of a wet six-row heat-pipe heat exchanger operating in tropical buildings," *International Journal of Energy Research*, vol. 27, no. 3, pp. 187-202, 2003. <https://doi.org/10.1002/er.867>.
- [44] L. J. Shah, "TRNSYS models of Evacuated Tubular Collectors," Danmarks Tekniske Universitet, 2005.
- [45] D. Brough, A. Mezquita, S. Ferrer, C. Segarra, A. Chauhan, S. Almahmoud, N. Khordehghah, L. Ahmad, D. Middleton, H. I. Sewell and H. Jouhara, "An experimental study and computational validation of waste heat recovery from a lab scale ceramic kiln using a vertical multi-pass heat pipe heat exchanger," *Energy*, vol. 208, 2020. <https://doi.org/10.1016/j.energy.2020.118325>.
- [46] V. Guichet and H. Jouhara, "Condensation, evaporation and boiling of falling films in wickless heat pipes (two-phase closed thermosyphons): A critical review of correlations," *Internal Journal of Thermofluids*, Vols. 1-2, February 2020. <https://doi.org/10.1016/j.ijft.2019.100001>.
- [47] V. Guichet, S. Almahmoud and H. Jouhara, "Nucleate pool boiling heat transfer in wickless heat pipes (two-phase closed thermosyphons): A critical review of correlations," *Thermal Science and Engineering Processes*, vol. 13, October 2019. <https://doi.org/10.1016/j.tsep.2019.100384>.
- [48] Engineers Field, "Flue Gas Properties," [Online]. Available: <https://engineersfield.com/flue-gases-properties-table-density-viscosity/>. [Accessed 16 July 2020].
- [49] The Engineering Toolbox, "Dry Air Properties," [Online]. Available: https://www.engineeringtoolbox.com/dry-air-properties-d_973.html. [Accessed 21 July 2020].

- [50] P. Evans, "Properties of water at atmospheric pressure," [Online]. Available: <https://theengineeringmindset.com/properties-of-water-atmospheric-pressure-saturated-liquid/>. [Accessed 21 July 2020].
- [51] Solutia, "Therminol 66," [Online]. Available: <http://twf.mpei.ac.ru/TTHB/HEDH/HTF-66.PDF>. [Accessed 16 July 2020].
- [52] J. Backhurst, J. Harker, R. J.F. and J. Coulson, Chemical Engineering Volume 1, Butterworth-Heinemann, 1999.
- [53] F. Kreith, R. Manglik and M. Bohn, Principles of Heat Transfer 7th ed., Stamford: Cengage Learning, Inc, 2011.
- [54] W. Khan, J. Culham and M. Yovanovich, "Convection heat transfer from tube banks in crossflow: Analytical approach," *International Journal of Mass Transfer*, pp. 4831-8, 2006. <https://doi.org/10.1016/j.ijheatmasstransfer.2006.05.042>.
- [55] A. Colburn, "A method of correlating forced convection heat transfer data and a comparison with fluid friction," *Transactions of the American Institute of Chemical Engineering*, pp. 174-210, 1933.
- [56] E. Grimison, "Correlation and utilization of new data on flow resistance and heat transfer for cross flow of gases over tube banks," *Transactions of the American Society of Mechanical Engineers*, pp. 583-94, 1937.
- [57] J. Holman, Heat Transfer 7th edition, New York: McGraw-Hill, 1992.
- [58] H. Hausen, Heat Transfer in Counter Flow, Parallel Flow and Cross Flow, New York: McGraw-Hill, 1983.
- [59] A. Zukauskas, "Heat transfer from tubes in crossflow," *Advanced Heat Transfer*, pp. 93-160, 1972.
- [60] P. Pongsoi, S. Pikulkajorn and S. Wongwises, "Heat transfer and flow characteristics of spiral fin-and-tube heat exchangers: A review," *International Journal of Heat and Mass Transfer*, no. 79, pp. 417-431, 2014. <https://doi.org/10.1016/j.ijheatmasstransfer.2014.07.072>.

- [61] T. Domański and K. Kmiecik, "Load-bearing capacity of the steel-to-timber connections in fire temperature," *MATEC Web of Conferences*, vol. 262, 2019. <https://doi.org/10.1051/mateconf/201926209005>.
- [62] University of Wisconsin-Madison. Solar Energy Laboratory, TRNSYS 17, Volume 7, Programmer's Guide, n.d..
- [63] B. Delpech, M. Milani, L. Montorsi, D. Boscardin, A. Chauhan, S. Almahmoud, B. Axcell and H. Jouhara, "Energy efficiency enhancement and waste heat recovery in industrial processes by means of the heat pipe technology: Case of the ceramic industry," *Energy*, vol. 158, pp. 656-65, 2018. <https://doi.org/10.1016/j.energy.2018.06.041>.